frontiers in Earth Science

ORIGINAL RESEARCH
published: 24 December 2021
doi: 10.3389/feart.2021.741789

# Acceleration of Dynamic Ice Loss in Antarctica From Satellite Gravimetry

*Theresa Diener[1,2], Ingo Sasgen[2]*, Cécile Agosta[3], Johannes J. Fürst[1], Matthias H. Braun[1], Hannes Konrad[4] and Xavier Fettweis[5]*

[1]Department of Geography and Geosciences, Institute of Geography, Friedrich-Alexander Universität Erlangen-Nürnberg, Erlangen, Germany, [2]Division of Glaciology, Alfred-Wegener-Institut Helmholtz-Zentrum Für Polar- und Meeresforschung, Bremerhaven, Germany, [3]Laboratoire des Sciences du Climat et de l'Environnement (LSCE), Gif-sur-Yvette, France, [4]Satellite-based Climate Monitoring, Deutscher Wetterdienst, Offenbach am Main, Germany, [5]Department of Geography, SPHERES research unit, University of Liège, Liège, Belgium

The dynamic stability of the Antarctic Ice Sheet is one of the largest uncertainties in projections of future global sea-level rise. Essential for improving projections of the ice sheet evolution is the understanding of the ongoing trends and accelerations of mass loss in the context of ice dynamics. Here, we examine accelerations of mass change of the Antarctic Ice Sheet from 2002 to 2020 using data from the GRACE (Gravity Recovery and Climate Experiment; 2002–2017) and its follow-on GRACE-FO (2018-present) satellite missions. By subtracting estimates of net snow accumulation provided by re-analysis data and regional climate models from GRACE/GRACE-FO mass changes, we isolate variations in ice-dynamic discharge and compare them to direct measurements based on the remote sensing of the surface-ice velocity (2002–2017). We show that variations in the GRACE/GRACE-FO time series are modulated by variations in regional snow accumulation caused by large-scale atmospheric circulation. We show for the first time that, after removal of these surface effects, accelerations of ice-dynamic discharge from GRACE/GRACE-FO agree well with those independently derived from surface-ice velocities. For 2002–2020, we recover a discharge acceleration of -5.3 ± 2.2 Gt $yr^{-2}$ for the entire ice sheet; these increasing losses originate mainly in the Amundsen and Bellingshausen Sea Embayment regions (68%), with additional significant contributions from Dronning Maud Land (18%) and the Filchner-Ronne Ice Shelf region (13%). Under the assumption that the recovered rates and accelerations of mass loss persisted independent of any external forcing, Antarctica would contribute 7.6 ± 2.9 cm to global mean sea-level rise by the year 2100, more than two times the amount of 2.9 ± 0.6 cm obtained by linear extrapolation of current GRACE/GRACE-FO mass loss trends.

**Keywords: Antarctica, GRACE/GRACE-FO, ice-dynamic discharge, surface mass balance, sea-level rise (SLR), mass balance, ISMIP6, climate indices**

OPEN ACCESS

***Edited by:***
*Thomas Vikhamar Schuler, University of Oslo, Norway*

***Reviewed by:***
*Jonathan L. Bamber, University of Bristol, United Kingdom*
*Anthony Mémin, Université Côte d'Azur, France*

****Correspondence:***
*Ingo Sasgen*
*ingo.sasgen@awi.de*

***Specialty section:***
*This article was submitted to Cryospheric Sciences, a section of the journal Frontiers in Earth Science*

***Received:*** *15 July 2021*
***Accepted:*** *29 November 2021*
***Published:*** *24 December 2021*

***Citation:***
*Diener T, Sasgen I, Agosta C, Fürst JJ, Braun MH, Konrad H and Fettweis X (2021) Acceleration of Dynamic Ice Loss in Antarctica From Satellite Gravimetry. Front. Earth Sci. 9:741789. doi: 10.3389/feart.2021.741789*

## 1 INTRODUCTION

One of the most profound consequences of global warming is the retreat of ice sheets and glaciers worldwide, with the exception of only a few locations (WCRP Global Sea Level Budget Group, 2018). The increasing atmosphere and ocean temperatures in the Arctic have led to substantial ice loss of Arctic glacier systems (Wouters et al., 2019). For the Greenland Ice Sheet, mass loss has exceeded mass gain by about 30% (Sasgen et al., 2020; Velicogna et al., 2020). In Antarctica, current mass loss

of grounded ice exceeds mass gain only by about 6%, yet it is progressively increasing (Shepherd et al., 2018; Rignot et al., 2019a). Satellite observations show ice-shelf thinning (Paolo et al., 2015) and collapse (Scambos, 2004) as well as ice-stream thinning and grounding line retreat, inducing changes that propagate far into the ice sheet's interior (Jenkins et al., 2018; Konrad et al., 2018; Shepherd et al., 2019). Models provide further evidence that such perturbations along the ice sheet margin can entail changes far inland (Fürst et al., 2016; Reese et al., 2018). Since the 1990s, enhanced ice shelf disintegration has occurred along the Antarctic Peninsula, reducing buttressing and causing acceleration of tributary glaciers (De Angelis, 2003; Silva et al., 2020). In the Amundsen Sea Embayment, West Antarctica, submarine melting, enhanced by upwelling of comparably warm Circumpolar Deep Water (Jenkins et al., 2018; Nakayama et al., 2018), has initiated thinning of ice shelves, leading to acceleration of grounded ice propagating inland, further perpetuating retreat and destabilization of the ice sheet in this region (Konrad et al., 2017; Selley et al., 2021). In East Antarctica, in contrast, changes in ice flow or ice shelf stability are less frequent; however, regional grounding line retreat is observed for Totten glacier (Li et al., 2015), while ice-shelf thickening is observed in some parts of Dronning Maud Land (Smith et al., 2020).

With a retrograde bedrock, below current sea level in most parts, West Antarctica is at risk for complete disintegration when ocean temperatures exceed certain thresholds (Sutter et al., 2016; Arthern and Williams, 2017). Simulations five centuries into the future have shown that West Antarctica may eventually contribute up to 3 m of global sea-level rise in high-impact, low-probability scenarios (DeConto and Pollard, 2016), with updated assessments indicating a likely contribution between -7.8 and 30.0 cm in the year 2100 for unmitigated climate change (Seroussi et al., 2020). Furthermore, projections show competing influences of increasing snow accumulation versus increasing ice-dynamic losses in future scenarios for the Antarctic Ice Sheet (Seroussi et al., 2020; Edwards et al., 2021). Separating mass loss acceleration caused by temporary variations in snow accumulation and sustained ice-dynamic trends in satellite observations, and connecting these changes to the respective underlying processes and drivers, is critical for evaluating risks of surpassing dynamical thresholds of ice sheet disintegration (Garbe et al., 2020).

During the past decades, advancements in satellite observation have remarkably improved our capability to monitor the mass balance state of the Antarctic Ice Sheet, augmenting sparse *in-situ* measurements. Radar and laser altimetry together with models of the snow and firn densification, as well as gravimetry measurements, facilitated differential estimates of mass change at regular time intervals (Shepherd et al., 2018). Equally important, interferometric radar enabled the determination of surface-ice velocities, providing estimates of the changes of the ice-dynamic discharge across the grounding line, representing the mass output of the ice sheet (Mouginot et al., 2014; Rignot et al., 2019a). Together with modelling estimates of the surface-mass balance, the mass input to the ice sheet, the mass balance of the Antarctic Ice sheet has been estimated by subtraction in the so-called mass budget method (Rignot et al., 2008). Using a suite of methods and satellite observations of altimetry, gravimetry and interferometry, the community produced a consensus estimate that the mass change of grounded ice in Antarctica tripled from -53 ± 29 Gt $yr^{-1}$ to -159 ± 26 Gt $yr^{-1}$ between 1992 and 2017 (Shepherd et al., 2018).

Here, we aim to estimate ice discharge based on the mass balance equation.

$$M(t) = SMB(t) + D(t) \tag{1}$$

where $SMB(t)$ is mass input to the ice sheet by the surface-mass balance cumulated over time, and $D(t)$ is mass output of the ice sheet by ice-dynamic discharge across the grounding line, also cumulated over time. Typically, $D(t)$ is measured by interferometric radar or speckle tracking and $SMB(t)$ is modelled to obtain the mass changes of the ice sheet $M(t)$ (Rignot et al., 1997; Rignot et al., 2008; Shepherd et al., 2018; Mankoff et al., 2020). Here, we solve for the cumulative ice-dynamic discharge $D(t)$, and in particular its acceleration, based on estimates of $SMB(t)$ provided by re-analysis data and regional climate models, as well as measurements of $M(t)$ from GRACE and GRACE-FO satellite data. We show for the first time that our indirect method of estimating acceleration of cumulative discharge yields results consistent with those inferred from measurements of the surface-ice velocity, with comparable uncertainties.

The outline of this paper is as follows. First, we describe the input data sets GRACE/GRACE-FO and SMB, along with their uncertainties. Next, we introduce the time series analysis performed on the data in order to recover accelerations of the mass change and their uncertainties. Then, we explain the assumptions underlying the extrapolation of the sea level contributions to the year 2100. After that, we present our estimates of the mass trends, the interannual mass changes and their relation to atmospheric circulation patterns, as well as the mean cumulative discharge rate. Finally, we present accelerations of cumulative discharge in comparison with published values, discuss their drivers and show implications for global sea level rise in the year 2100.

# 2 MATERIALS AND METHODS

## 2.1 GRACE/GRACE-FO Data

We estimate mass changes of the Antarctic Ice Sheet from 2002 to 2020 based on data from the GRACE (2002–2017) and the GRACE-FO (launched 2018, operational) satellite missions that provide nearly continuous monthly measurements of the time-varying gravity field of the Earth. Based on the Stokes potential coefficients (Level-2 data) issued by the missions' Science Data System (SDS), which are a spherical harmonic representation of the Earth's gravity field changes, mass redistribution on the Earth surface can be derived (Tapley et al., 2004, 2019). We use Release 06 (RL06) Level-2 data from the three GRACE/GRACE-FO SDS teams; German Research Centre for Geosciences (GFZ) (Dahle et al., 2019), Centre for Space Research University of Texas, Austin,

United States (CSR) (Bettadpur, 2018; Save, 2019) and Jet Propulsion Laboratory, California Institute of Technology (JPL) (Yuan, 2019), as well their combination (AV RL06) (Sasgen et al., 2020). A comparison of time series of mass change obtained from the four Level 2 GRACE/GRACE-FO data sets is shown in **Supplementary Figure S1**.

The data capture 191 out of 218 possible months during the missions' operation; 163 monthly solutions from GRACE covering April 2002 to June 2017 and 28 solutions from GRACE-FO covering June 2018 to November 2020. To estimate uncertainties in the derived mass change time series associated with processing choices and corrections, we additionally consider Level-3 mass change gridded products for Antarctica provided by the Technical University of Dresden (TUD) published *via* the GravIS data portal (Sasgen et al., 2019a) and the CSR RL06 Mascons (Save et al., 2016). All GRACE/GRACE-FO Level 2 and 3 data used in this study are publicly available (Data availability).

## 2.2 Inversion for Mass Change

We invert the monthly GRACE/GRACE-FO gravity fields for mass changes in Antarctica using a spectral inversion method similar to Jacob et al. (2012), modifying the forward modelling approach in the spatial domain previously applied to Antarctica (Sasgen et al., 2013). For this, we define spatial patterns of mass change, from either satellite observations or modelling, within 25 drainage basins of the ice sheet (**Figure 1**), calculate their spectral gravity field signature, and adjust these spectra by scaling in order to minimize the difference to the observed spectrum represented by the GRACE/GRACE-FO Stokes coefficients. Prior to adjustment, we limit the representation of the GRACE/GRACE-FO coefficients to the region of Antarctica by employing a spectral mask of the ice sheet using a buffer zone of 200 km (Martinec, 1989). Finally, we obtain the total mass change within in each drainage basin by spatial integration of the scaled mass distribution underlying the forward models. The optimal adjustment factors are estimated by weighted least-squares, allowing us to account for the noise structure in the data set of GRACE/GRACE-FO coefficients.

We compose a forward model by assuming that the spatial pattern of mass change corresponds to CryoSat-2 rates of mass change (Sasgen et al., 2019b) for trends and accelerations, and the mean surface mass balance (van Wessem et al., 2018) for the remaining, de-trended temporal components. We find that evaluating GRACE/GRACE-FO data at the basin scale is relatively insensitive to the mass distribution underlying the forward model. We quantify the uncertainty of our results associated with these processing choices by comparing with the independently derived Level-3 mass change products TUD COST-G (Sasgen et al., 2019a) and the CSR RL06 Mascons (Save et al., 2016) (Data availability). A sensitivity analysis using a spectral circular mask extending from the South Pole to 60°S, as well as using no masking produces consistent results.

An advantage of the spectral inversion method is that uncertainties of the GRACE/GRACE-FO coefficients can be used directly as weighting factors in the least-squares adjustment without propagation to the spatial domain. Here, we estimate these uncertainties of the GRACE/GRACE-FO coefficients from the root-mean squared residual of each coefficient's time series. We note that the spectral inversion estimates are very similar to previous results performed in the spatial domain (Sasgen et al., 2013; Sasgen et al., 2019b), however, show a slightly lower noise level and better agreement with the expected fluctuations of the surface mass balance. The results fall within the range of a multi-source ensemble of GRACE mass balances for Antarctica undertaken as part of the Ice Sheet Mass Balance Inter-Comparison Exercise (IMBIE2) (Shepherd et al., 2018) (**Supplementary Figure S2**).

As a final step, we correct the trends of mass change for each basin for the signal induced by glacial-isostatic adjustment (GIA) using the arithmetic average of the models IJ05 R2 (Ivins et al., 2013), AGE1 (Sasgen et al., 2013) and ICE-6G_D (Peltier et al., 2015) (**Supplementary Figure S3**). These GIA models are a subset of the larger ensemble investigated for the IMBIE2 (Shepherd et al., 2018) and selected as they have shown to reproduce GPS-inferred uplift rates in Antarctica (Martín-Español et al., 2016), except for high uplift rates measured in the Amundsen Sea Embayment region (Barletta et al., 2018). At the same time, the models are constructed using independent approaches and largely different input data (**Supplementary Table S2** in Shepherd et al., 2018), allowing us to reflect regional variability in the GIA patterns. In addition, it has been shown that applying this GIA correction produces GRACE mass rates consistent with CryoSat-2 mass rates for the time period 2011–2017 (Sasgen et al., 2019b). As the consistency with GPS-inferred uplift rates implies similar response magnitudes and patterns, the uncertainty of GIA derived from the model differences is smaller compared to the full IMBIE2 ensemble.

We acknowledge two limitations related to our GIA correction. First, regional optimized models with improved fit to the GPS uplift rates exist for the Amundsen Sea Embayment region (Barletta et al., 2018), the Antarctic Peninsula (Nield et al., 2014), and the Siple Coast (Nield et al., 2016), yielding GIA-induced apparent mass changes of 17 Gt $yr^{-1}$, 3 Gt $yr^{-1}$, and a range of ±6–8 Gt $yr^{-1}$, respectively. However, these predictions are based on regional Earth structure models and cannot be simply superimposed with continent-wide GIA simulations adopting a global average Earth structure. Moreover, it has been shown that adopting a thin elastic lithosphere may produce large localized uplift rates without a large impact on the gravity field change at the spatial resolution of GRACE/GRACE-FO (Sasgen et al., 2017). However, we note that mass loss rates in the Amundsen Sea Embayment region could be underestimated by 10 Gt $yr^{-1}$ to 14 Gt $yr^{-1}$ Barletta et al. (2018).

Another limitation is the assumption that GIA is approximately linear over short time periods and has henceforth no impact on accelerations measured with GRACE/GRACE-FO. Barletta et al. (2018) have shown that for Amundsen Sea Embayment region, underlain by a low-viscous upper mantle, the GIA rate increases over time. The authors state an increase of the GIA rates of about 2% per year, equivalent to a per year increase of the GIA-induced apparent rate of mass change of +0.3 Gt $yr^{-1}$. However, the acceleration of

GIA in this region remains an issue of investigation, as it strongly depends on the poorly known load changes during the past century. In addition, adding the effect of this local response based on a specific viscosity structure to the continent-wide GIA corrections would introduce an inconsistency we can not resolve within this study.

## 2.3 Uncertainty of GRACE/GRACE-FO Mass Change

We estimate the uncertainty of the monthly GRACE/GRACE-FO mass changes at the basin scale from two components; the time varying, normalized noise level of the GRACE/GRACE-FO gravity field solutions, and the residual variability of the mass change within each basin. To obtain the noise level of each monthly solution, we calculate the coefficient's residual time series $C_{jm}^{Res}(t_i)$ after removing bias, trend, acceleration, annual, and semi-annual and temporal variations longer than 4 months (using a moving average filter). Then, we cumulate the degree power of the residual in the noise-dominated spectral range 40–60, $\sum_{j=40}^{60}\sum_{m=-j}^{j}C_{jm}^{Res}(t_i)$. Finally, we normalize the cumulative degree power by the respective mean of all solutions, meaning that low-quality solutions show noise levels larger than one, high-quality solution lower than one. Then, we apply this time dependent noise factor to the root-mean-squared residual variability of mass change within each drainage basin. The resulting monthly uncertainty estimates for the SDS data sets (GFZ RL06, CSR RL06 and JPL RL06) and their combination (AV RL06) used for error propagation when estimating trends and accelerations (**Supplementary Figure S4**).

Apart from the stochastic noise associated with the GRACE/GRACE-FO coefficients, long-term mass changes may contain systematic differences arising from processing choices, background models and corrections, such as the GIA correction (Martín-Español et al., 2016; Shepherd et al., 2018) or the ocean and atmosphere de-aliasing during Level-2 data processing (Dobslaw et al., 2017; Hardy et al., 2017). Here, we empirically estimate the uncertainty of the trends and accelerations from the differences of our mass change time series with the publicly available Level-3 mass change products TUD COST-G (Sasgen et al., 2019a) and the CSR RL06 Mascons (Save et al., 2016) (Data availability). To increase the sample size, we estimate the linear trend and acceleration by randomly selecting 163 out of 191 monthly solutions from each data set and repeating this procedure 1,000 times in a bootstrap approach. In addition, we estimate the uncertainty of the GIA adjustment correction based on the standard deviation of model realizations entered into IMBIE2 (Shepherd et al., 2018) (**Supplementary Figure S3**). The total uncertainty of the GRACE/GRACE-FO trend and acceleration components is estimated as the quadratic sum of the respective propagated monthly uncertainties (stochastic) and the cross-solution empirical uncertainties, including uncertainties of the correction for GIA in the linear trend component (systematic). The standard deviations of the linear trends and accelerations and their stochastic and systematic components are shown in **Supplementary Figure S5**.

## 2.4 Surface Mass Balance

We approximate the SMB over the grounded part of the Antarctic Ice Sheet by net accumulation, calculated as total snowfall, minus snowmelt and evaporation based on the reanalyses product ERA-5 of the European Centre for Medium-Range Weather Forecasts (ECMWF) for the time period January 1979 to September 2020 (Copernicus Climate Change Service, 2017). The data are provided on a regular $0.25^{\circ} \times 0.25^{\circ}$ geographic grid, yielding a spatial resolution of approximately 15 km along the coast of West Antarctica (latitude ~73°S). In addition, we use 35 km × 35 km output of regional climate model MARv3.6 (Agosta et al., 2019) for quantifying uncertainties related to the surface mass balance component (see following section). In contrast to the Greenland Ice Sheet, which experiences extensive summer melt, snowfall constitutes almost the entire surface-mass balance over grounded ice in Antarctica. Our analysis of ERA-5 data shows that snowmelt amounts to less than 1% of the regionally averaged surface mass balance, with some exception along the Antarctic Peninsula (up to 4%), confirming previous results (Lenaerts et al., 2012; Agosta et al., 2019). We estimate storage changes as measured by GRACE/GRACE-FO by integrating monthly estimates of SMB, hereafter referred to as cumulative SMB, $SMB(t)$, over the time periods 2002–2017 and 2002–2020, respectively. The cumulative SMB is summed up within each basin or region (**Figure 1**).

## 2.5 Uncertainty of Surface Mass Balance

We estimate the uncertainty of cumulative SMB based on four model realizations, which involve the ERA-5 reanalysis and three MARv3.6 simulations with different lateral forcing (ECMWF ERA-Interim, MERRA2 and JRA-55) (Agosta et al., 2019). Thus, the uncertainty derived from this ensemble encompasses deviations in the large-scale atmosphere circulation, as well as inherent modelling differences. We separate the uncertainty analysis into three temporal components, reflecting differences between de-trended monthly estimates, the linear trend and the acceleration of the cumulative SMB estimates, respectively. The differences are analyzed for moving 15-years time windows within the time period covered by all four realizations (1979–2015). While deviations of detrended monthly cumulative SMB estimates tend to reflect random fluctuations introduced by differences in the atmosphere forcing and climate modeling, deviations of long-term changes (e.g., trends and accelerations) will arise from potential biases and different sensitivities in the responses of the models to the same forcing. Thus, similar to the GRACE/GRACE-FO analysis, we consider the random monthly uncertainties of ±55 Gt (**Supplementary Figure S4**) and their propagated uncertainties of the trends and accelerations (hereafter named stochastic; $\pm 10\ \mathrm{Gt\ yr^{-1}}$ and $\pm 0.5\ \mathrm{Gt\ yr^{-2}}$, respectively). As a second component, we estimate systematic uncertainties of the SMB trends and accelerations, amounting to $\pm 9\ \mathrm{Gt\ yr^{-1}}$ and $\pm 0.4\ \mathrm{Gt\ yr^{-2}}$, respectively (**Supplementary Figure S5**). The total uncertainty is obtained by quadratic summation of the propagated monthly and the systematic uncertainties.

## 2.6 Time Series Analysis

For each basin, we decompose the time series of mass change from GRACE/GRACE-FO and cumulative SMB using least-squares linear regression with a quadratic temporal model consisting of offset, $\bar{M}$, linear trend, $\dot{M}$, and acceleration, $\ddot{M}$,

$$\hat{M}(t) = \frac{1}{2}\ddot{M}t^2 + \dot{M}t + \bar{M} \quad (2)$$

In the regression, we employ time variable (stochastic) monthly uncertainties for GRACE/GRACE-FO, which reduces the influence of low-quality monthly solutions, for example at the end of the GRACE mission in 2017 (**Supplementary Figure S4**). We assume constant uncertainties and therefore equal weighting for the monthly cumulative SMB estimates, in the absence of representative time-variable monthly uncertainties. Note that throughout this paper, accelerations are presented as the temporal derivative of the rates (factor 1/2 in **Eq. 2**).

The offset $\bar{M}$ in **Eq. 2** reflects the mean mass distribution on and within the Earth in the region of Antarctica, which is not of interest here. The respective linear trend $\dot{M}$ represents the average rate of mass change either of the ice sheet (GRACE/GRACE-FO), the rate of cumulative SMB or the rate of cumulative discharge, $\dot{SMB}(t)$ and $\dot{D}(t)$, respectively. The acceleration term $\ddot{M}$ in the GRACE/GRACE-FO time series represents, depending on the sign, a long-term decrease or increase of the mass balance of the ice sheet. The acceleration of cumulative SMB, $\ddot{SMB}$, indicates trends in the rate of mass input, caused by changes in the rate of snowfall accumulation due to atmospheric variability and climate trends. The residual of the GRACE/GRACE-FO mass change and quadratic fit of **Eq. 2**, $M(t) - \hat{M}(t)$, is dominated by mass changes related to interannual SMB variability in addition to noise. Although dynamic discharge may show year-to-year variability for individual glaciers and ice streams, these fluctuations are below the detection limit of GRACE/GRACE-FO, more so because regional averaging further reduces the possibly uncorrelated variability within a larger entity.

## 2.7 Grouping Basins Into Regions

The comparison of GRACE/GRACE-FO mass changes, $M(t)$, and cumulative SMB mass changes, $SMB(t)$, shows very high correlation and agreement in magnitude at interannual time scales (**Supplementary Figure S6**), providing justification for calculating discharge by differencing both data sets. To further increase the robustness of our results, we group the 25 basins to ten regions as shown in **Figure 1**, effectively decreasing the spatial resolution and, thus, noise in the GRACE/GRACE-FO data. For this, we identify blocks of co-varying interannual changes of the cumulative SMB, as reflected by inter-basin correlations (**Supplementary Figure S7**). These covariations are a consequence of a common regional atmospheric forcing causing synchronous fluctuations and regional multi-year trends in snow accumulation (Mémin et al., 2015), discussed later in this paper.

## 2.8 Discharge Estimate and Uncertainties

The mass changes $M(t)$ of the Antarctic Ice Sheet result from the difference between the cumulative surface mass balance $SMB(t)$ minus the cumulative ice discharge over the grounding line $D(t)$ (Rignot et al., 1997, 2008; Shepherd et al., 2018; Mankoff et al., 2020). Here, we reorder the mass balance equation (**Eq. 1**), to estimate cumulative discharge as $D(t) = M(t) - SMB(t)$, where $M(t)$ is obtained from GRACE/GRACE-FO, and $SMB(t)$ is obtained from the snow accumulation product of the re-analysis data (ERA-5). In the following, we focus on the long-term temporal components for specific time periods; namely the rate and acceleration of cumulative discharge, $\dot{D}$ and $\ddot{D}$, respectively, and likewise its rate and acceleration of cumulative SMB, $\dot{SMB}$ and $\ddot{SMB}$, respectively.

For fast-flowing ice streams and fixed geometries, $\dot{D}$ is proportional to the surface-ice velocity (Rignot et al., 1997, 2008; Mankoff et al., 2020), therefore an increase in surface-ice velocity implies a component of accelerated discharge $\ddot{D}$. On the other hand, an acceleration of $SMB(t)$ may reflect both long term and temporary trends in the snowfall rate, for example, due to increased moisture content in the atmosphere or prevailing circulation, respectively. We estimate the rates and accelerations independently for the time series of $M(t)$ and $SMB(t)$ and infer accelerations of $D(t)$ by subtraction. Uncertainties of the trends and accelerations of $M(t)$ and $SMB(t)$ are added to obtain uncertainties of the respective temporal component of $D(t)$ (**Supplementary Figure S5**).

Note that $SMB(t)$ is defined as positive if adding mass to the ice sheet system; it has positive values for all basins. Therefore, a positive acceleration of $SMB(t)$ denotes an increase in mass gain, indicated by a positive regression coefficient for the acceleration. Likewise, $D(t)$ is defined as positive if adding mass to the ice sheet system and has negative values for all basins. In the following, an acceleration of $D(t)$ refers to an increase in mass loss out of the system, indicated by a negative regression coefficient for the acceleration. The mass change of the ice sheet $M(t)$, can have either sign. Therefore, we specify an increase in mass loss, as acceleration of mass loss (negative regression coefficient), a reduction in mass loss as deceleration (positive regression coefficient). In this definition, an acceleration in $SMB(t)$ can compensate an acceleration in $D(t)$ in terms of mass loss $M(t)$.

We compare rates and accelerations of $D(t)$ obtained with the indirect method with estimates based on surface-ice velocity measurements (Rignot et al., 2019a), referred to as "direct" estimates. As basin definitions slightly differ between both estimates, we map the direct estimates onto our basins by scaling with the respective area, in the few cases of intersecting basins. For consistency, we limit the evaluation period to the common time interval 2002–2017, for which we calculate the unweighted mean of the annual rates of cumulative discharge from the direct method (Rignot et al., 2019a).

## 2.9 Extrapolation of Sea-Level Contribution

In the following, we will extrapolate sea level rise caused by the recovered mass balance trends and ice-dynamic accelerations

to the year 2100 (here; 80 years). As a sensitivity experiment, we distinguish between the extrapolation based on the GRACE/GRACE-FO mass balance $\dot{M}$ only, and the extrapolation additionally including acceleration of the cumulative discharge, $D(t)$, denoted $\ddot{D}$, obtained by the indirect method. We evaluate the temporal model of **Eq. 2** and extrapolate the total mass change to the year 2100,

$$M_t(t) = \frac{1}{2}\ddot{D}t^2 + \dot{M}t \quad (3)$$

The quadratic extrapolation is supported by Ice Sheet Model Intercomparison 6 (ISMIP6) of the Coupled Model Intercomparison Project Phase 6 (CMIP6) projections of Antarctica's contribution to sea-level rise until the year 2100, which suggest a time evolution well-approximated by a second-order polynomial, across models and model set ups, as well as using various climate forcing (Payne et al., 2021). Note, however, that despite similar temporal characteristics of the projections, the complex interplay of physical processes in response to the climate forcing governs the actual path of each simulation. We chose to extrapolate to the year 2100 as the typical time frame of ice sheet model projections. In addition, (Lowry et al., 2021), show that ice-sheet model projections forced by RCP2.6 and RCP8.5 scenarios become significantly different only after 2100 (at the 68% confidence level).

We would like to emphasize limitations of this extrapolation. First, mass balance and dynamic acceleration are assumed to prevail unchanged until the end of this century, implying no changes in the external forcing. Next, we neglect possible long-term changes in SMB, which have been shown to have an important impact on the sea-level contribution Payne et al. (2021). In addition, we extrapolate present-day mass balance components based on a relatively short time period of 19 years. Wouters et al. (2013) have estimated the uncertainty in mass trend estimates due to stochastic variability of the Antarctic Ice Sheet as function of observation length. For the contribution of SMB and a 19-years time series, Wouters et al. (2013) estimate a stochastic variability of $\pm 3.4\ \mathrm{Gt\ yr^{-2}}$ for the acceleration (denoted according to **Eq. 2**) and $\pm 3.9\ \mathrm{Gt\ yr^{-1}}$ for the rates (**Figure 3** in Wouters et al., 2013). In addition, the authors suggest a contribution from ice dynamic variability an order of magnitude lower. The uncertainty of the rates ($\pm 3.9\ \mathrm{Gt\ yr^{-1}}$) and the dynamic acceleration ($\pm 0.3\ \mathrm{Gt\ yr^{-2}}$, denoted according to **Eq. 2**) caused by stochastic variability is added to the propagated uncertainties of the indirect method in the extrapolation of the sea-level contribution. Note that the uncertainty in the extrapolation is based only on the propagation of the uncertainty of the presented-day trends and accelerations; it does not included process-related uncertainties, which could possibly be estimated in a Monte Carlo approach based on the CMIP6 output. In the following, we assume a volume density of water of $997\ \mathrm{kg\ m^{-3}}$ and the area of the ocean of $361{\cdot}10^6\ \mathrm{km^2}$, such that 360 Gt of ice-mass loss causes 1 mm of global mean sea-level rise.

# 3 RESULTS

## 3.1 Antarctic Ice-Mass Balance in the GRACE/GRACE-FO Period

Regional mass changes and their associated linear trends are estimated based on 191 monthly GRACE and GRACE-FO gravity solutions for the Antarctic Ice Sheet (**Figure 2**). For the entire ice sheet, rates of mass change, $\dot{M}$, amount to -131 ± 23 $\mathrm{Gt\ yr^{-1}}$, of which -138 ± 8 $\mathrm{Gt\ yr^{-1}}$ originate from West Antarctica, -17 ± 9 $\mathrm{Gt\ yr^{-1}}$ from the Antarctica Peninsula and +24 ± 20 $\mathrm{Gt\ yr^{-1}}$ from East Antarctica. Within the study period from April 2002 to September 2020, the ice sheet contributed approximately 6 mm to global mean sea level rise.

The three main subdivisions of the Antarctic Ice Sheet (**Figure 1**) show different mass evolutions. The year 2009 marks a transition to mass gain in East Antarctica, continuing until 2012, and increased loss rates in West Antarctica (**Figure 2**). The mass gain in East Antarctica is mainly a consequence of high precipitation events in Dronning Maud Land (Boening et al., 2012) (**Supplementary Figure S6**), cancelling out the increasing losses in West Antarctica after 2009 in the mass balance of the whole ice sheet. Apart from long-term trends, all regions exhibit substantial interannual fluctuations (**Supplementary Figure S6**). East Antarctica contributes the most to the interannual fluctuations of the entire ice sheet, which appear random, however, reflect the superposition of asynchronous mass signals arising from accumulation variability within smaller regions of this largest part of Antarctica, discussed later. In contrast, the mass balance in West Antarctica dominates the mass loss signal of the entire Antarctic Ice Sheet (-138 ± 23 $\mathrm{Gt\ yr^{-1}}$ versus -131 ± 8 $\mathrm{Gt\ yr^{-1}}$, respectively), with an additional contribution from the Antarctic Peninsula.

## 3.2 Interannual Mass Changes due to Snow Accumulation

Next, we investigate the interannual variations of the mass changes $M(t)$ from GRACE/GRACE-FO and $SMB(t)$, obtained as residual after removal of the fitted temporal model $\hat{M}(t)$ shown in **Eq. 2** (offset, linear and quadratic trends). For the entire Antarctic Ice Sheet $M(t) - \hat{M}(t)$ from GRACE/GRACE-FO and the cumulative SMB show a Pearson correlation coefficient of 0.59, well above the 95% significance level of 0.30 accounting for auto-correlation, which reduces the effective degrees of freedom (Barker et al., 2016). Applying a three-month moving average filter reduces short-term GRACE/GRACE-FO monthly fluctuations, which are not present in the SMB time series and therefore likely associated with noise. This increases the correlation to 0.72 at a significance level of 0.40 (including autocorrelation). After application of the moving average, the temporal characteristics of $M(t)$ from GRACE/GRACE-FO and $SMB(t)$ are highly consistent (**Supplementary Figure S6**); therefore, we refrain from similar filtering of the SMB time series.

At the basin scale, including the 3-month moving average (**Supplementary Figure S6**), correlations lie above 0.8 for twelve

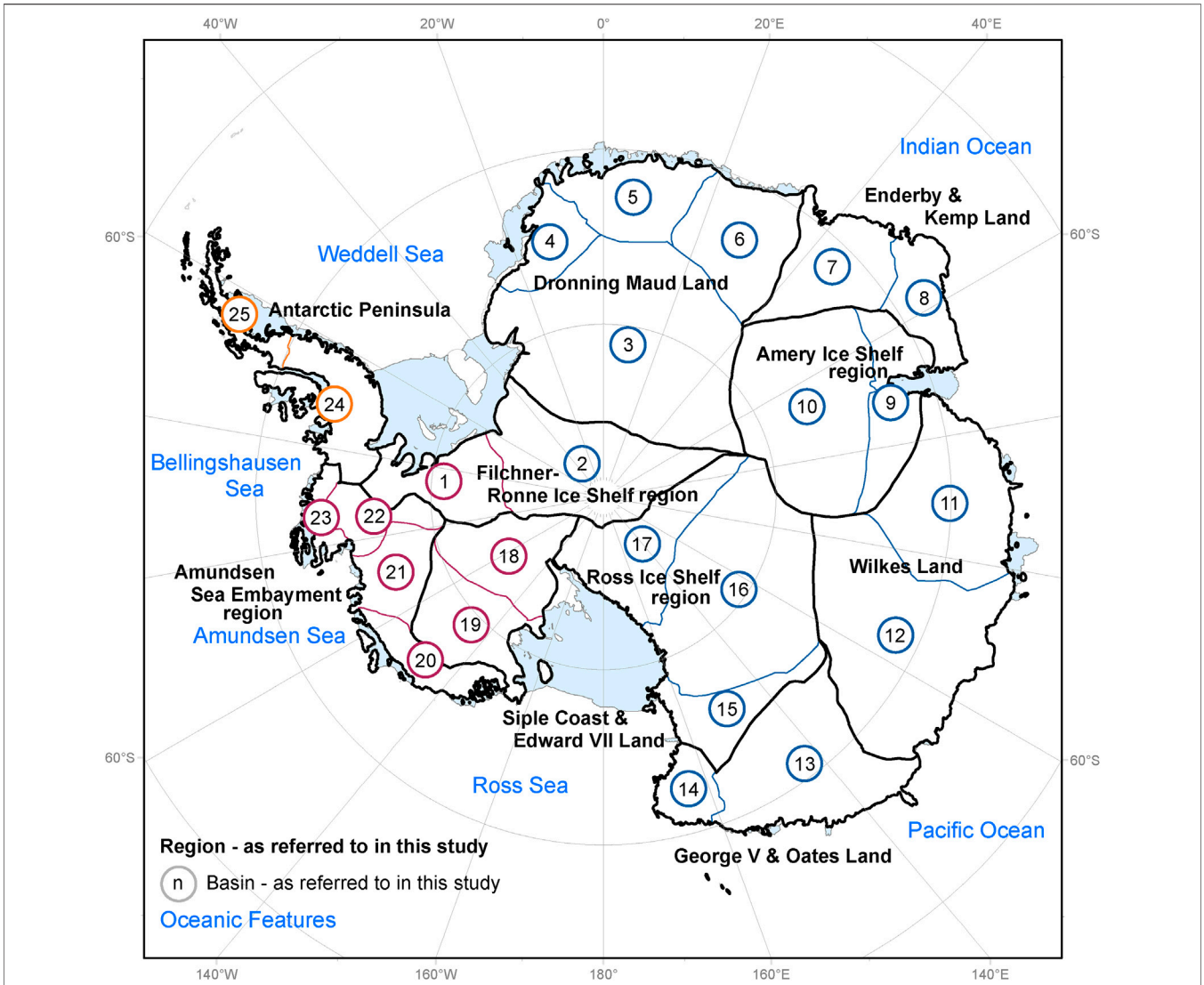


**FIGURE 1 |** Drainage basins and regional division of the Antarctic Ice Sheet. The continental Antarctic Ice Sheet is divided into 25 drainage basins following Sasgen et al. (2013). The basins are further grouped into ten larger entities (regions), named according to their characteristic geographical feature, such as the adjacent ocean embayment or ice shelf (black lines). The basins are attributed to East Antarctica (blue lines), West Antarctica (red lines) and the Antarctic Peninsula (yellow lines). Labels locate geographic features discussed in the text. The projection is Polar Stereographic centered at 90°S and 0°E, with the true latitude of 71°S and WGS84 (EPSG: 3031).

of the 25 basins. These basins show a large magnitude of the SMB variability with respect to GRACE/GRACE-FO uncertainties. We identify two regions where de-trended GRACE/GRACE-FO mass changes correlate remarkably well with SMB fluctuations; basins 20 through 24 in the Amundsen and Bellingshausen Sea Embayment region (coefficient >0.92) and basins 4 through 8 in Dronning Maud Land (coefficient >0.85). Highly correlated, with coefficients above 0.83, are basins 11 through 13 in East Antarctica, while remaining basins show moderate correlation. For example coefficients for basins 14 through 17, adjacent to the Ross Sea, range between 0.38 and 0.64. A likely reason is that magnitudes of variation in SMB$(t)$ are lower in these basins, leading to a smaller signal-to-noise ratio in the GRACE/GRACE-FO time series. Similar conditions may apply to basins 9 and 10 (Amery Ice Shelf region), even though here, correlations are typically greater than 0.62. We note that without filtering, correlations decrease on average by 0.07.

## 3.3 Discharge Rates From the Indirect Method

Rates of cumulative discharge, $\dot{D}$, obtained for 2002–2017 are consistent between the indirect and the direct method at the regional scale (**Figure 3**); for the entire Antarctic Ice Sheet and four out of ten regions, values agree within their respective uncertainties. However, in six regions, deviations exceed the

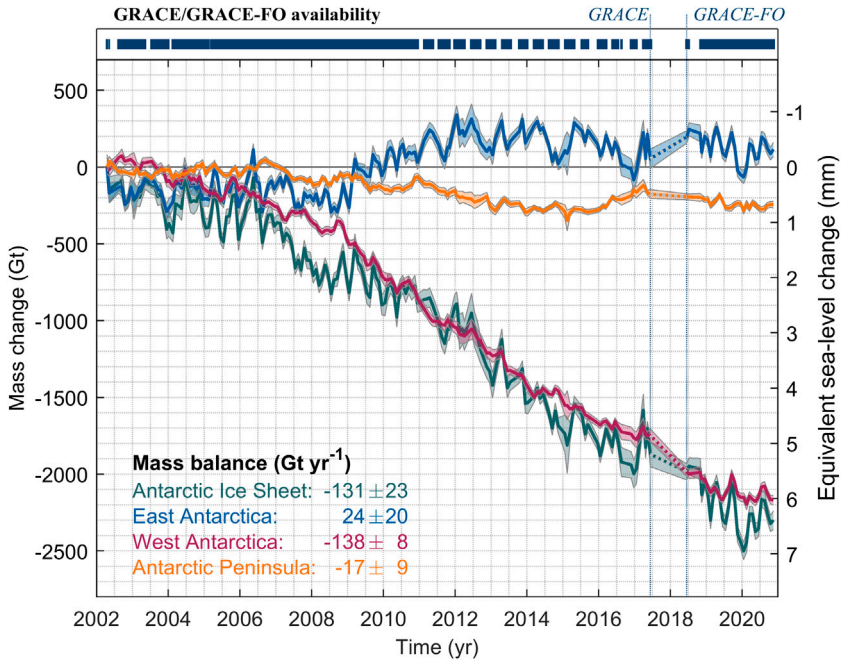


**FIGURE 2 |** Mass change of the Antarctic Ice Sheet from April 2002 to September 2020. Time series of mass change from the GRACE and GRACE-FO missions, $M(t)$, for the entire Antarctic Ice Sheet (green) and its division into East Antarctica (blue), West Antarctica (red) and the Antarctic Peninsula (yellow). The vertical lines indicate the end of the GRACE and begin of the GRACE-FO monthly data availability (June 2017 and July 2018, respectively). Shadings represent 1-$\sigma$ uncertainties. Equivalent sea-level contribution (right axis) is approximated as 1 mm sea-level rise for 360 Gt of ice mass loss.

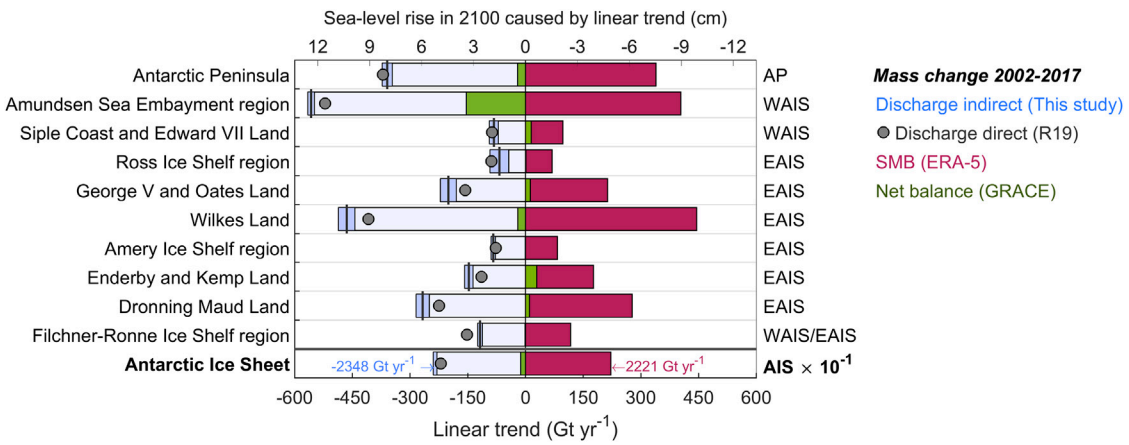


**FIGURE 3 |** Rate of mass change and its components for ten regions in Antarctica for 2002 to 2017. The rate of mass change, $\dot{M}$, from GRACE/GRACE-FO (green) is decomposed into the mean rate of the cumulative surface mass balance (SMB), $\dot{SMB}$, estimated from ERA-5 (red) and mean rate of cumulative discharge, $\dot{D}$ (blue), obtained by the difference between GRACE/GRACE-FO and the SMB component, along with its 1-$\sigma$ uncertainties (darker blue). For comparison, grey circles indicate direct estimates of the rate of cumulative discharge obtained from surface-ice velocities (R19) (Rignot et al., 2019a). Values for the entire Antarctic Ice Sheet are scaled by a factor of $10^{-1}$ for plotting. Rates of mass change are represented as Gt yr$^{-1}$ (bottom axis) and as integrated contribution to sea-level change by 2100 in cm (top axis). We assume 360 Gt of mass loss raise global mean sea level by 1 mm. Uncertainties for each component and the direct discharge estimate (Data availability) are shown in **Supplementary Figure S5**.

uncertainty ranges, possibly due to underestimated uncertainties of the SMB component in the indirect method. The median relative uncertainty for all regions is 5% for the SMB component, adding up to a relative uncertainty of the rates of cumulative discharge of 7% for the indirect method, compared to approximately 1% stated for the direct method.

For 2002–2020, we obtain an average annual surface mass balance, $\dot{SMB}$ based on ERA-5 snow accumulation minus snow melt and snow evaporation of 2228 ± 44 Gt yr$^{-1}$, comparing well

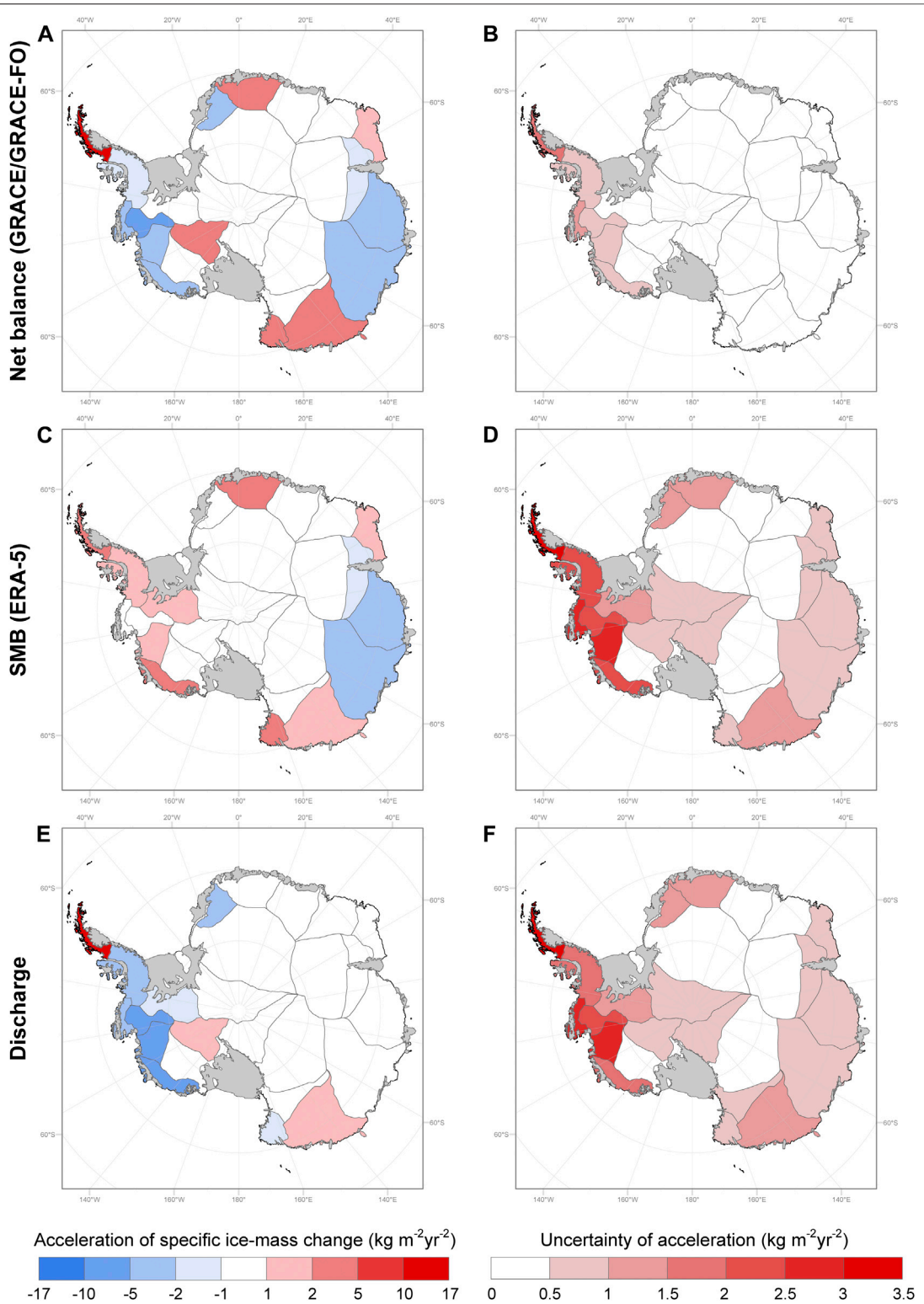


**FIGURE 4 |** Acceleration of mass change and its components for 25 drainage basins in Antarctica between 2002 and 2020. Shown are the accelerations of **(A)** mass change $\ddot{M}$ (GRACE/GRACE FO), **(C)** the cumulative surface mass balance, $\ddot{SMB}$ (ERA-5) and **(E)** cumulative ice-dynamic discharge, $\ddot{D}$ (indirect method), based on the difference between GRACE/GRACE-FO and the SMB component, along with their respective 1-σ uncertainties in **(B,D,F)**. Acceleration (blue) and deceleration (red) caused by a respective mass loss increase and mass gain increase are represented as change of specific mass balance (kg $m^{-2}$ $yr^{-2}$). The time period is April 2002 to September 2020. Accelerations and decelerations are denoted according to **Eq. 2** (factor ½). Note that a non-linear colorbar is chosen in **(A,C,E)** to emphasize signals of smaller magnitude. Results of the *t*-Test for significance are indicated in **Supplementary Table S1**. The projection is Polar Stereographic centered at 90°S and 0°E, with the true latitude of 71°S and WGS84 (EPSG:3031).

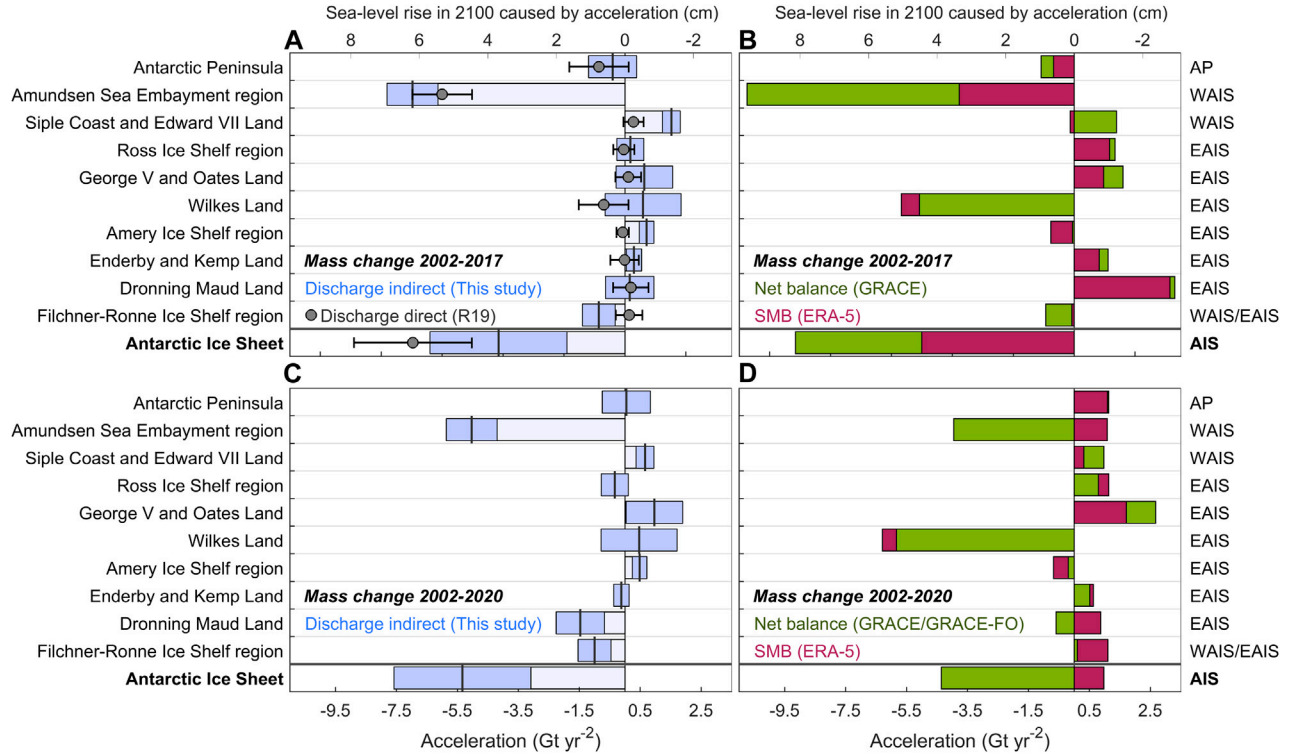


**FIGURE 5 |** Acceleration of cumulative ice-dynamic discharge for ten regions in Antarctica. **(A)** The acceleration of cumulative discharge, $\ddot{D}$, from the indirect method (this paper; blue) is compared to published values based of the direct method of (Rignot et al., 2019a) (R19; circles), and, related to **(B)** acceleration of mass change, $\ddot{M}$ (green), and acceleration of cumulative surface mass balance, $\ddot{SMB}$ (red), for the time period 2002 to 2017. **(C,D)** exhibit results for the extended time period 2002 to 2020 (no data from the direct method available). Uncertainty ranges reflect 1-$\sigma$ standard deviations. Values for the entire Antarctic Ice Sheet are scaled by a factor of $10^{-1}$ for plotting. Mass change values are represented as Gt yr$^{-2}$ (bottom axis; denoted according to **Eq. 2**) and as extrapolated contribution to sea-level change by 2100 in cm (top axis), assuming 360 Gt of mass loss raise global mean sea level by 1 mm. Uncertainties for each component and the direct discharge estimate (Data availability) are shown in **Supplementary Figure S5**. Results of the *t*-Test for significance are indicated in **Supplementary Table S2**.

with published values of 2098 ± 133 Gt yr$^{-1}$ for the time period 1979 to 2008 using a different regional climate model (Rignot et al., 2019a). Note that a two to three times larger relative uncertainty of SMB (10–15%; equal to ±88 to ±132 Gt yr$^{-1}$ for the entire ice sheet, respectively) would reconcile the indirect and direct discharge estimates within uncertainties for all regions, as would seven times larger discharge uncertainties of the direct method (7%; equal to ±62 Gt yr$^{-1}$).

## 3.4 Discharge Accelerations From the Indirect Method

In the following, we present basin-scale estimates of the acceleration of the mass change from GRACE/GRACE-FO, $SMB(t)$ approximated by ERA-5 net snow accumulation, as well as $D(t)$ calculated as difference of both observations for the time period 2002–2020. The spatial distribution of accelerations in each component ($\ddot{M}$, $\ddot{SMB}$ and $\ddot{D}$) is shown in **Figure 4** (2002–2020), displayed as average specific mass change within each basin (mass change divided by basin area), enabling a size-independent comparison of imbalances between basins.

### 3.4.1 GRACE/GRACE-FO Mass Change

The GRACE/GRACE-FO data recover dominant accelerations of mass change $\ddot{M}$ (increasing losses) in the Amundsen Sea Embayment region in West Antarctica, as well as Wilkes Land and the Amery Ice Shelf region, and, rather isolated, western Dronning Maud Land in East Antarctica (**Figure 4**) for the time period 2002–2020. The largest deceleration of mass loss per basin area (increasing mass gain) is detected for the northern Antarctic Peninsula. However, this observation is possibly a result of limitations of our approach concerning spatial resolution of GRACE/GRACE-FO and discussed later. Other regions with deceleration of mass loss are George V and Oates Land, as well as eastern Dronning Maud Land (**Figure 4**).

### 3.4.2 Surface-Mass Balance

In contrast to the mass change, SMB exhibits less heterogeneous acceleration estimates in 2002–2020, with positive values of $\ddot{SMB}$ (increasing mass gain) in most parts of Antarctica. An exception is Wilkes Land, where snowfall rates decreased within the time period, reducing the cumulative SMB, and causing mass loss increasing by -6.3 ± 1.2 Gt yr$^{-2}$ (basins 11 and 12). Overall, we obtain a positive, yet statistically not significant, acceleration of

$\ddot{SMB}$ (increasing mass gain) of +1.0 ± 2.5 Gt yr$^{-2}$ in the sum over the entire ice sheet, where moderately positive values of about +1 Gt yr$^{-2}$ in the majority of basins compensate the Wilkes Land negative exception. We find that the inferred values strongly depend on the time period due to the large regional fluctuations in the cumulative SMB caused by varying snow accumulation (**Supplementary Figure S6**). For example, considering the time period of 2002–2017, synchronous to the estimates of the direct method, atmospheric circulation has caused deceleration of the cumulative SMB (increasing mass loss) of -5.0 ± 2.2 Gt yr$^{-2}$ for the entire ice sheet (see also **Figure 5**).

### 3.4.3 Ice-Dynamic Discharge

The acceleration of $D(t)$ estimated by GRACE/GRACE-FO mass change minus $SMB(t)$ (indirect method; uncertainties are obtained by quadratic summation) is prevalent in West Antarctica. In Wilkes Land, increasing mass loss observed by GRACE/GRACE-FO prove to be almost entirely associated with an apparent deceleration of $SMB(t)$ (**Figure 4**), despite, for example, the reported mass loss of the Totten Glacier catchment (Li et al., 2016) and a negative mass balance obtained from GRACE/GRACE-FO (**Figure 3**). Moderate acceleration values of $\ddot{D}$ (increase in mass loss) are estimated for the Filchner-Ronne Ice Shelf region (basins 1 and 2; -1.0 ± 1.1 kg m$^{-2}$ yr$^{-2}$ and -0.9 ± 0.6 kg m$^{-2}$ yr$^{-2}$), Dronning Maud Land (basin 4; -2.4 ± 1.3 kg m$^{-2}$ yr$^{-2}$), as well as the eastern part of George V and Oates Land (basin 14; -1.1 ± 1.0 kg m$^{-2}$ yr$^{-2}$). Marked decelerations (positive values of $\ddot{D}$) are recovered only for the Siple Coast including the well-documented, decelerating Ice Streams B and C (Joughin, 2002) (basin 18; +1.7 ± 0.7 kg m$^{-2}$ yr$^{-2}$), as well as for the western part of George V and Oates Land (basin 13; +1.5 ± 1.2 kg m$^{-2}$yr$^{-2}$). The largest deceleration of +11.8 ± 3.4 kg m$^{-2}$ yr$^{-2}$ is detected for the northern Antarctic Peninsula (basin 25), which may be caused by resolution limitations in GRACE/GRACE-FO and SMB data and needs further investigation.

The dominant uncertainty in our indirect estimate of the cumulative discharge acceleration is introduced by uncertainties of the SMB component, typically between ±0.2 Gt yr$^{-2}$ and ±0.4 Gt yr$^{-2}$ for each basin (**Supplementary Figure S5**). These exceed uncertainties of the GRACE/GRACE-FO accelerations by a factor of about three for all basins. However, there are differences in the patterns of the uncertainties from GRACE/GRACE-FO and the SMB component (**Figure 4**). The GRACE/GRACE-FO uncertainties are introduced mainly by stochastic uncertainties of the GRACE/GRACE-FO coefficients (**Supplementary Figure S5**), known to increase towards lower latitudes. Consequently, basins covering areas further away from the pole show larger uncertainties. In contrast, SMB uncertainties are largest in high-accumulation areas such as coastal West Antarctica, pointing to systematic, signal-dependent uncertainties, inferred from the differences between SMB models (**Supplementary Figure S5**). Therefore, accelerations of cumulative discharge estimated by the indirect method depend critically on the accuracy of the SMB component and similar analysis will profit from future model developments (Mottram et al., 2020).

# 4 DISCUSSION

## 4.1 Antarctic Ice-Mass Balance in the GRACE/GRACE-FO Period

Concerning rates of mass change, $\dot{M}$, our estimates based the spectral inversion approach using combined GRACE/GRACE-FO solutions (**Supplementary Figure S1**) are in agreement with those based on published mass change products using different inversion approaches and input solutions. For example, the total mass balance of -131 ± 23 Gt yr$^{-1}$ is in good agreement with the independent estimates based on gridded products; -116 ± 23 Gt yr$^{-1}$ for CSR RL06 Mascons (Save et al., 2016) and -123 ± 23 Gt yr$^{-1}$ for TUD COST-G (Sasgen et al., 2019a). Furthermore, our mass balance falls within the range of gravimetric estimates from IMBIE2 (Shepherd et al., 2018) for the coincident time interval 2003–2016, for example -123 ± 23 Gt yr$^{-1}$ (this study) compared to -114 ± 33 Gt yr$^{-1}$ (IMBIE2) for the entire ice sheet (**Supplementary Figure S4**). Our results are more negative than a recent estimate of the mass balance of -99 ± 57 Gt yr$^{-1}$ for April 2002 to September 2019 (Velicogna et al., 2020), yet show agreement within uncertainties. Note that neither of these studies consider the regional GIA response in the Amundsen Sea Embayment region presented by Barletta et al. (2018) thus, possibly underestimating mass loss by 10 Gt yr$^{-1}$ to 14 Gt yr$^{-1}$.

## 4.2 Atmospheric Circulation Patterns and Snow Accumulation

To show the impact of atmospheric circulation patterns in the Southern Hemisphere on the interannual mass changes presented earlier, we now calculate temporal correlations with climate indices. In particular, we investigate the Southern Oscillation Index (SOI) (Parker, 1983) and the Southern Annular Mode (SAM) (Thompson, 2002), reflecting atmosphere pressure differences, as well as the NIÑO 3.4/4 indices, derived from gradients in sea-surface temperatures in the central Pacific (Trenberth, 1975). Previous studies have shown correlation of these indices with monthly rates of precipitation in Antarctica (Turner, 2004). As we analyze storage changes of the ice sheet represented by cumulative sums of monthly fluxes, we cumulate the indices analogous to the processing of the SMB data to enable a direct comparison.

The cumulative SMB, $SMB(t)$, and the cumulative indices exhibit groups of basins with correlated variations, similar to the mass changes between basins presented earlier (**Supplementary Figure S7**). Correlations cluster as blocks of negative and positive values. For example, the correlation with the SOI is negative for the Filchner-Ronne Ice Shelf region (basins 1 and 2), positive for the Dronning Maud Land region (basins 3 through 6), negative for the George V and Oates Land region (basins 13 and 14) and the Siple Coast eastward up to and including the Amundsen Sea Embayment region (basins 18 through 23). These correlations are above the 95% significance level (considering auto-correlation). The indices of NIÑO 3.4/4 based on sea-surface temperatures show largely the same pattern of covariance, however, with opposite sign owing to the strong anti-correlation of SOI and

NIÑO 3.4/4 (**Supplementary Figure S7**) (Cullather et al., 1996). Fluctuations in relation to the SAM are visible mainly for central Dronning Maud Land, large parts of the ice sheet draining into the Amundsen Sea Embayment and the northern Antarctic Peninsula (**Supplementary Figure S7**). Although these correlations with individual indices are significant, we note that their superposition may describe the complex modes of atmospheric circulation and their effect on the SMB variability more accurately (Fogt and Bromwich, 2006; Mémin et al., 2015; Kaitheri et al., 2021). Furthermore, Mémin et al. (2015) and Kaitheri et al. (2021) suggest additional modulation of SMB anomalies related to the Antarctic Circumpolar Wave, propagating the climate anomalies eastward around Antarctica at a period of six to eight years.

The results show that interannual variations of $SMB(t)$ and their correlations with atmospheric conditions are an important non-stationary temporal signal in the GRACE/GRACE-FO time series. In particular, the asynchronous modulation of snowfall anomalies between Dronning Maud Land and the Amundsen Sea Embayment region (**Supplementary Figure S6** and **Supplementary Figure S7**) is part of global atmosphere variability closely linked to the El Niño Southern Oscillation (Zhang et al., 2021). For short time scales, changes in rates of mass change between East and West Antarctica are considerably driven by the SMB component (for example in 2009; **Figure 2**) and should not be misinterpreted as a persistent shift in ice dynamics.

## 4.3 Comparison of the Direct and Indirect Acceleration Estimates

For the entire Antarctic Ice Sheet, as well as for eight out of the ten regions, accelerations of cumulative discharge obtained in this study show agreement with the independent direct estimates within uncertainties between 2002 and 2017 (Rignot et al., 2019b) (**Figure 5**). Largest values of acceleration of $D(t)$ (increasing mass loss) are detected for the Amundsen Sea Embayment region, amounting to a value of $\ddot{D}$ of -5.0 ± 0.8 Gt yr$^{-2}$, well in line with the direct estimates. Exceptions from the overall agreement of direct and indirect estimates are Siple Coast and Edward VII Land, for which we estimate a deceleration $\ddot{D}$ of +0.7 ± 0.3 Gt yr$^{-2}$, somewhat larger than that obtained from the direct approach (+0.3 ± 0.3 Gt yr$^{-2}$). For the Filchner-Ronne Ice Shelf region, we detect an acceleration of $cD(t)$ of -1.0 ± 0.5 Gt yr$^{-2}$ not present in the direct estimates (+0.1 ± 0.4 Gt yr$^{-2}$). For both regions, cumulative SMB does not remove the decelerations and accelerations prominent in the GRACE data, leading to non-zero values for cumulative discharge in 2002–2017.

We further investigate the robustness of our approach to recover the quasi-stationary accelerations of $D(t)$ by prolonging the time period to 2020, now including GRACE-FO data. **Figure 5** illustrates that values of $\ddot{D}$ only moderately change within their uncertainties, when including about three more years of data (2002–2020). In contrast to the stability of the discharge estimates, accelerations of GRACE/GRACE-FO mass change $M(t)$ and, prominently, $SMB(t)$ show considerable variations when using different time periods. For example, GRACE/GRACE-FO recover considerably different magnitudes of accelerating mass loss in the Amundsen Sea Embayment region in both periods. For the SMB components, accelerations estimates $S\ddot{M}B$ even differ in sign. Similarly, for the entire ice sheet, acceleration of GRACE/GRACE-FO mass loss is larger in 2002–2017 compared to 2002–2020, while the estimated acceleration value $\ddot{D}$ remains mostly unchanged, due to subtraction of different SMB contributions. This further supports our finding that it is possible to separate slow-varying discharge changes from SMB-induced fluctuations in the GRACE/GRACE-FO data.

In contrast to the uncertainties of the rates of $D(t)$ discussed earlier (**Figure 3**), uncertainties of the acceleration estimates $\ddot{D}$ are of similar magnitude for the direct and indirect methods. While possible biases in the absolute amount of snow accumulation limit the precision of the indirect discharge rates $\dot{D}$, as they determine the mean rate of $SMB(t)$, accelerations are influenced by uncertainties in the temporal trends of snow accumulation. In addition, for the discharge rates $\dot{D}$, the GIA correction of the GRACE/GRACE-FO is an important source of systematic uncertainty (**Supplementary Figure S5**), while it is much less important when considering accelerations $\ddot{D}$.

## 4.4 Relation to Drivers of Changing Ice Discharge

Our study locates the largest acceleration of $D(t)$ (increase in mass loss) in the *Amundsen Sea Embayment region* (**Figure 5**), in accordance with prior studies (Sutterley et al., 2014; Gardner et al., 2018) and analysis using direct observations (Rignot et al., 2019a). In this region, various observations indicate that the ice sheet is in a state of transition, with the risk of exceeding the instability threshold related to the Marine Ice Sheet Instability (DeConto and Pollard, 2016; Sutter et al., 2016).

For many glacier systems, retreating and thinning ice shelves have triggered fundamental ice-dynamic responses. For example, the mass loss of the Getz Ice Shelf (adjacent to basin 20) was followed by an increase in the velocity of the tributary glaciers in the period of 2007–2013, as well as dynamic glacier thinning and grounding line retreat between 2010 and 2013 (Joughin et al., 2014; Rignot et al., 2014; Chuter et al., 2017; Gardner et al., 2018). An increase in ice discharge by 6% is determined for the Pine Island, Thwaites, Haynes, Pope, Smith and Kohler Glaciers between 2008 and 2015, which equals an acceleration of -2.4 Gt yr$^{-2}$ (Gardner et al., 2018), somewhat lower than in this study (basins 21 and 22; -3.1 ± 0.7 Gt yr$^{-2}$). Overall, our estimates of cumulative discharge acceleration are in line with the increase of 77% in this sector from 1973 to 2013 (Rignot et al., 2019a).

In basins 1 and 2 of the *Filchner-Ronne Ice Shelf region*, we detect moderate acceleration of $D(t)$ between 2002 and 2017 (-0.9 ± 0.5 Gt yr$^{-2}$; **Figure 5**), in contrast to the direct estimate of +0.1 ± 0.4 Gt yr$^{-2}$ (Rignot et al., 2019a). Although accelerations remain negative using GRACE/GRACE-FO data of CSR RL06 Mascons or TUD COST-G, we cannot exclude possible biases in the gravimetry data caused by long-term tidal-aliasing signals, known to be a source of uncertainty in the area of the large ice shelves in Antarctica (Dobslaw et al., 2017).

For the *Antarctic Peninsula*, our results show no significant change in ice-dynamic discharge, which is in contrast to the direct estimates, indicating moderate acceleration (**Figure 5**). At the basin scale, we identify discharge deceleration (+1.3 ± 0.4 Gt yr$^{-2}$) in northern and acceleration (-1.2 ± 0.7 Gt yr$^{-2}$) in the southern part of the Antarctic Peninsula (**Figure 4**). Evaluating GRACE/GRACE-FO data over this elongated and narrow region is challenging and may be subject to biases introduced by processing choices, even though our analysis using published mass change products CSR RL06 Mascons and TUD COST-G yields consistent results. In addition, estimates of the SMB component could be biased due to the limited resolution of the ERA-5 re-analysis data. This could be clarified in future studies using higher resolution products. However, projections suggest that glacier discharge is substantially less sensitive to collapse of the Larsen C Ice Shelf along the northern Peninsula (basin 25) than the southern George IV Ice Shelf (basin 24) (Schannwell et al., 2018). Less frequent events of ice shelf disintegration compared to the 1990s are possibly related to incipient near-surface temperature cooling (Turner et al., 2016), even though most observations indicate increasing discharge for both basins (Wouters et al., 2015; Cook et al., 2016; Hogg et al., 2017).

In contrast to most of West Antarctica, cumulative discharge decelerates along the *Siple Coast and Edward VII Land* (basins 18 and 19; +0.7 ± 0.3 Gt yr$^{-2}$) feeding the Ross Ice Shelf. During the last 4 decades, glaciers along the Siple Coast showed reduced ice flow (Rignot et al., 2019a) and experienced mass gain between 1992 and 2017 (Schröder et al., 2019). The Whillans Ice Stream is anticipated to slow down (Joughin et al., 2005), and stagnate by 2070 (Thomas et al., 2013), in-line with a discharge deceleration of 25.3% during 1997 and 2009, when including the adjacent Mercer Ice Stream (Gardner et al., 2018). The reduction in ice velocity is not only present near the grounding line, where the mass loss finally occurs, but reaches a few hundred kilometers inland (Scheuchl et al., 2012).

The *Ross Ice Shelf region* in East Antarctica (basins 15 through 17) include complex terrain of the Transantarctic Mountains (Fretwell et al., 2013). For this region, our estimates of acceleration $\ddot{D}$ are close to zero, indicating ice-dynamic stability, enabled by a topography of broad and stabilizing ridges (Morlighem et al., 2020).

*George V and Oates Land* (basins 13 and 14) show moderate dynamic deceleration, $\ddot{D}$, after removal of large SMB-driven accelerations from the GRACE/GRACE-FO data (+1.0 ± 0.9 Gt yr$^{-2}$; **Figure 5**). Our estimate are in line with previous studies, finding no pronounced glacier retreat between 1972 and 2013 for both basins (Lovell et al., 2017).

For *Wilkes Land* (basins 11 and 12), East Antarctica, we identify no significant acceleration of $D(t)$, despite a mass loss increase of -5.8 ± 0.2 Gt yr$^{-2}$ observed by GRACE/GRACE-FO and mean rates of cumulative discharge being among the largest in Antarctica (2002–2020: -465 ± 22 Gt yr$^{-1}$; **Figure 3**). Mass and elevation change within basin 12 (**Figure 1**), including Totten Glacier, are well documented in previous studies (Schröder et al., 2019), however reflect spatially confined changes close to the coast (Shepherd et al., 2019). Acceleration of $M(t)$ (increase in mass loss) detected with GRACE/GRACE-FO is almost completely caused by a decline in snow accumulation ($\ddot{SMB}$ is -6.3 ± 1.2 Gt yr$^{-2}$ for 2002–2020), as part of a strong interannual variation in this region. In contrast to our estimate, studies have shown a 40% increase of dynamic discharge in 2017 compared to 1979–2003 (Rignot et al., 2019a), as well as a loss of grounded ice (Smith et al., 2020). The future evolution of this part of the ice sheet critically depends on the evolution of the Totten Glacier, due to its large catchment area and retrograde bedrock slope, promoting instability similar to West Antarctica (Gomez et al., 2010; Durand and Pattyn, 2015; Greenbaum et al., 2015). Comparable conditions apply to the Denman Glacier (Brancato et al., 2020; Smith et al., 2020; Miles et al., 2021). It is the consensus that the evolution of heat transport due to changing ocean currents and ocean temperatures will have a decisive impact on this marine-based part of the ice sheet (Rintoul et al., 2016; Levermann et al., 2020). It will be important to reconcile the observational data sets in order to reliably quantify the dynamic changes in this region, holding high potential of sea-level rise.

The *Amery Ice Shelf region* exhibits only small values of dynamic acceleration $\ddot{D}$ (+0.5 ± 0.2 Gt yr$^{-2}$), but also of $\ddot{SMB}$ (-0.7 ± 0.2 Gt yr$^{-2}$), indicating relative dynamic stability and a low influence of mass change by atmospheric circulation, particularly in the interior part (basin 10). Our finding is supported by unchanging ice velocities since 1970 (Rignot et al., 2019a) and observation of slight deceleration in ice flow from 1968 to 2014 (Tong et al., 2018).

*Enderby Land and Kemp Land* (basins 7 and 8) show no sign of acceleration of cumulative discharge in the investigation period, in agreement with direct observations (**Figure 5**). However, for Dronning Maud Land (basins 3 through 6) we isolate an acceleration of -1.5 ± 0.8 Gt yr$^{-2}$ for $D(t)$, which is similar for both time periods investigated, despite a large variation in the SMB component (**Figure 5**). We note that mass changes obtained from altimetry (Schröder et al., 2019) are consistent with GRACE/GRACE-FO. Therefore, we expect accelerations to be of similar magnitude and sign using altimetry instead of gravimetry data.

## 4.5 Extrapolated Sea-Level Contribution From Antarctica

Next we extrapolate the present-day mass balance (-131 ± 23 Gt yr$^{-1}$) together with the acceleration of $D(t)$ (-5.3 ± 2.2 Gt yr$^{-2}$) for a time period of 80 years, to explore the relevance of the quadratic term of today's mass balance for the future sea-level rise contribution from Antarctica. Assuming 360 Gt of mass loss to be equivalent to 1 mm of sea-level rise and applying **Eq. 3**, we obtain a sea-level contribution of 7.6 ± 2.9 cm by the year 2100. Note that we have included an additional uncertainty of ±0.4 Gt yr$^{-2}$ associated with the stochastic variably of ice discharge, as inferred by Wouters et al. (2013). This sea-level contribution is more than two times the amount obtained by extrapolating only the linear trend of the mass balance (2.9 ± 0.5 cm), highlighting the sensitivity of the future sea-level contributions to ice-dynamic accelerations. Adopting non-linear GIA correction for the GRACE/GRACE-FO data of +0.6 Gt yr$^{-2}$ (Barletta et al., 2018) would further increase the acceleration of cumulative discharge to -6.0 ± 2.2 Gt yr$^{-2}$, resulting in a sea-level contribution of 8.0 ± 2.9 cm by 2100.

The extrapolation including accelerations yields with 7.6 ± 2.9 cm a sea-level contribution that lies within the medium range of -8 and 30 cm of CMIP5/ISMIP6 projections for unmitigated climate change (Seroussi et al., 2020) and the CMIP6/ISMIP6 ensemble evaluation of Edwards et al. (2021), projecting likely contribution between -5 and 14 cm by year 2100. Lowry et al. (2021) show that limiting projections to trajectories satisfying present-day observations considerably reduces the ensemble spread caused by uncertainties in model parameters, for example related to ice rheology and sliding. As the uncertainty of the present-day observations expressed as sea-level rise in 2100 (±2.9 cm) is considerably lower than the ensemble spread, we expect that evaluating the projection ensembles with observed trends and accelerations will further confine the range of likely trajectories.

We emphasize the severe limitation that our extrapolation assumes constant rate of $SMB(t)$ until the year 2100. Projections have shown that long-term changes in snow accumulation related to a higher moisture content in the warming atmosphere may compensate dynamic losses, potentially leading to net mass gain of the ice sheet and an associated fall in sea level (Seroussi et al., 2020). However, the spread in projected SMB is large due to differences in forcing, models and downscaling (Payne et al., 2021), and further research is needed to quantify the relative importance of SMB, ice-dynamic changes and their interaction in projections of sea-level rise. Our results show that it is possible to separate superimposed substantial multi-year fluctuations in the SMB component from ice-dynamic changes in GRACE/GRACE-FO data. We consider such an isolation in current satellite data an essential first step for model validation and calibration, in order to reduce uncertainties in projections of the future sea-level contribution from the Antarctic Ice Sheet.

## 5 CONCLUSION

The mass evolution of the Antarctic Ice Sheet is a crucial factor for projecting future sea level rise. We have investigated accelerations of mass change $\ddot{M}$ from GRACE/GRACE-FO and the cumulative surface mass balance $S\ddot{M}B$ based on re-analysis data to determine, by differencing, acceleration in cumulative discharge, $\ddot{D}$, in Antarctica between 2002 and 2020. We have shown that our acceleration estimates obtained by this indirect method, represent an independent alternative to direct estimates from surface-ice velocities (Rignot et al., 2019a), producing consistent magnitudes and comparable uncertainties. We find that the main limiting factor of the indirect method is the systematic uncertainty in the surface mass balance estimates, exceeding GRACE/GRACE-FO uncertainties by a factor of about three. However, the spatial resolution of the satellite gravimetry data poses limitations for estimates of smaller basins, such as the northern Antarctic Peninsula. Furthermore, we have shown that mass changes caused by snowfall variability strongly superimpose with signals from dynamic acceleration in the GRACE/GRACE-FO data. Separating the surface-mass balance and ice discharge variations in differential satellite measurements is a crucial first step for evaluating ice sheet models and extrapolating future sea-level change.

Assuming that acceleration of cumulative discharge and current rates of mass loss are persistent features in Antarctica, we obtain, by extrapolation, a contribution of 7.6 ± 2.9 cm of the ice sheet to global mean sea level rise by the year 2100. Our extrapolation to 2100 falls within with the range of -5–14 cm of sea-level rise obtained from larger CMIP6/ISMIP6 ensembles of numerical projections (Edwards et al., 2021), indicating the potential of present-day trend and acceleration estimates to further tighten the range of plausible model trajectories (Lowry et al., 2021). We conclude that satellite monitoring is essential for identifying the current evolution pathway of Antarctica, offering a valuable constraint on complex projections of future sea-level rise.

## DATA AVAILABILITY STATEMENT

The raw data supporting the conclusion of this article will be made available by the authors, without undue reservation.

## AUTHOR CONTRIBUTIONS

TD and IS developed the study and carried out the data analysis. CA and XF provided MAR model output and provided input to the SMB analysis. JJF supported the detailed analysis with regard to ice-dynamic adjustment and the interpretation of ice-discharge variations. MHB provided input to the regional analysis of the Antarctic Peninsula. HK provided input to the regional analysis of West and East Antarctica. All authors contributed the writing and editing of the paper.

## FUNDING

IS acknowledges funding by the Helmholtz Climate Initiative REKLIM (Regional Climate Change), a joint research project of the Helmholtz Association of German Research Centres (HGF), as well as support by the Open Access Publication Funds of Alfred-Wegener-Institut Helmholtz-Zentrum für Polar-und Meeresforschung.

## ACKNOWLEDGMENTS

The authors kindly thank Jonathan L. Bamber and Anthony Mémin for their constructive comments that have helped us improve our manuscript. Further, we thank Thomas Vikhamar Schuler for additional comments and his editorial assistance in the publication process.

## SUPPLEMENTARY MATERIAL

The Supplementary Material for this article can be found online at: https://www.frontiersin.org/articles/10.3389/feart.2021.741789/full#supplementary-material

## REFERENCES


Agosta, C., Amory, C., Kittel, C., Orsi, A., Favier, V., Gallée, H., et al. (2019). Estimation of the Antarctic Surface Mass Balance Using the Regional Climate Model MAR (1979-2015) and Identification of Dominant Processes. *The Cryosphere* 13, 281–296. doi:10.5194/tc-13-281-2019

Arthern, R. J., and Williams, C. R. (2017). The Sensitivity of West Antarctica to the Submarine Melting Feedback. *Geophys. Res. Lett.* 44, 2352–2359. doi:10.1002/2017GL072514

Barker, L. J., Hannaford, J., Chiverton, A., and Svensson, C. (2016). From Meteorological to Hydrological Drought Using Standardised Indicators. *Hydrol. Earth Syst. Sci.* 20, 2483–2505. doi:10.5194/hess-20-2483-2016

Barletta, V. R., Bevis, M., Smith, B. E., Wilson, T., Brown, A., Bordoni, A., et al. (2018). Observed Rapid Bedrock Uplift in Amundsen Sea Embayment Promotes Ice-Sheet Stability. *Science* 360, 1335–1339. doi:10.1126/science.aao1447

Bettadpur, S. (2018). GRACE UTCSR Level-2 Processing Standards Document for Level-2 Product Release 0006. Available at: ftp://isdcftp.gfz-potsdam.de/grace/DOCUMENTS/Level-2/GRACE_CSR_L2_Processing_Standards_Document_for_RL06.pdf.

Boening, C., Lebsock, M., Landerer, F., and Stephens, G. (2012). Snowfall-driven Mass Change on the East Antarctic Ice Sheet. *Geophys. Res. Lett.* 39, L21501. doi:10.1029/2012gl053316

Brancato, V., Rignot, E., Milillo, P., Morlighem, M., Mouginot, J., An, L., et al. (2020). Grounding Line Retreat of Denman Glacier, East Antarctica, Measured with COSMO-SkyMed Radar Interferometry Data. *Geophys. Res. Lett.* 47, e2019GL086291. doi:10.1029/2019GL086291

Chuter, S. J., Martín-Español, A., Wouters, B., and Bamber, J. L. (2017). Mass Balance Reassessment of Glaciers Draining into the Abbot and Getz Ice Shelves of West Antarctica. *Geophys. Res. Lett.* 44, 7328–7337. doi:10.1002/2017GL073087

Cook, A. J., Holland, P. R., Meredith, M. P., Murray, T., Luckman, A., and Vaughan, D. G. (2016). Ocean Forcing of Glacier Retreat in the Western Antarctic Peninsula. *Science* 353, 283–286. doi:10.1126/science.aae0017

Copernicus Climate Change Service (2017). ERA5: Fifth Generation of ECMWF Atmospheric Reanalyses of the Global Climate. Copernicus Climate Change Service Climate Data Store (CDS), Date of Access. Available at: https://cds.climate.copernicus.eu/cdsapp#!/home (Accessed November 4, 2019).

Cullather, R. I., Bromwich, D. H., and Van Woert, M. L. (1996). Interannual Variations in Antarctic Precipitation Related to El Niño-Southern Oscillation. *J. Geophys. Res.* 101, 19109–19118. doi:10.1029/96JD01769

Dahle, C., Murböck, M., Flechtner, F., Dobslaw, H., Michalak, G., Neumayer, K., et al. (2019). The GFZ GRACE RL06 Monthly Gravity Field Time Series: Processing Details and Quality Assessment. *Remote Sensing* 11, 2116. doi:10.3390/rs11182116

De Angelis, H., and Skvarca, P. (2003). Glacier Surge after Ice Shelf Collapse. *Science* 299, 1560–1562. doi:10.1126/science.1077987

DeConto, R. M., and Pollard, D. (2016). Contribution of Antarctica to Past and Future Sea-Level Rise. *Nature* 531, 591–597. doi:10.1038/nature17145

Dobslaw, H., Bergmann-Wolf, I., Dill, R., Poropat, L., Thomas, M., Dahle, C., et al. (2017). A New High-Resolution Model of Non-tidal Atmosphere and Ocean Mass Variability for De-aliasing of Satellite Gravity Observations: AOD1B RL06. *Geophys. J. Int.* 211, 263–269. doi:10.1093/gji/ggx302

Durand, G., and Pattyn, F. (2015). Reducing Uncertainties in Projections of Antarctic Ice Mass Loss. *The Cryosphere* 9, 2043–2055. doi:10.5194/tc-9-2043-2015

Edwards, T. L., Nowicki, S., Marzeion, B., Hock, R., Goelzer, H., Seroussi, H., et al. (2021). Projected Land Ice Contributions to Twenty-First-century Sea Level Rise. *Nature* 593, 74–82. doi:10.1038/s41586-021-03302-y

Fogt, R. L., and Bromwich, D. H. (2006). Decadal Variability of the ENSO Teleconnection to the High-Latitude South Pacific Governed by Coupling with the Southern Annular Mode*. *J. Clim.* 19, 979–997. doi:10.1175/JCLI3671.1

Fretwell, P., Pritchard, H. D., Vaughan, D. G., Bamber, J. L., Barrand, N. E., Bell, R., et al. (2013). Bedmap2: Improved Ice Bed, Surface and Thickness Datasets for Antarctica. *Cryosphere Discuss.* 7, 375. doi:10.5194/tcd-6-4305-2012

Fürst, J. J., Durand, G., Gillet-Chaulet, F., Tavard, L., Rankl, M., Braun, M., et al. (2016). The Safety Band of Antarctic Ice Shelves. *Nat. Clim Change* 6, 479–482. doi:10.1038/nclimate2912

Garbe, J., Albrecht, T., Levermann, A., Donges, J. F., and Winkelmann, R. (2020). The Hysteresis of the Antarctic Ice Sheet. *Nature* 585, 538–544. doi:10.1038/s41586-020-2727-5

Gardner, A. S., Moholdt, G., Scambos, T., Fahnstock, M., Ligtenberg, S., van den Broeke, M., et al. (2018). Increased West Antarctic and Unchanged East Antarctic Ice Discharge over the Last 7 Years. *The Cryosphere* 12, 521–547. doi:10.5194/tc-12-521-2018

Gomez, N., Mitrovica, J. X., Tamisiea, M. E., and Clark, P. U. (2010). A New Projection of Sea Level Change in Response to Collapse of marine Sectors of the Antarctic Ice Sheet. *Geophys. J. Int.* 180, 623–634. doi:10.1111/j.1365-246X.2009.04419.x

Greenbaum, J. S., Blankenship, D. D., Young, D. A., Richter, T. G., Roberts, J. L., Aitken, A. R. A., et al. (2015). Ocean Access to a Cavity beneath Totten Glacier in East Antarctica. *Nat. Geosci* 8, 294–298. doi:10.1038/ngeo2388

Hardy, R. A., Nerem, R. S., and Wiese, D. N. (2017). The Impact of Atmospheric Modeling Errors on GRACE Estimates of Mass Loss in Greenland and Antarctica. *J. Geophys. Res. Solid Earth* 122, 10,440–10,458. doi:10.1002/2017JB014556

Hogg, A. E., Shepherd, A., Cornford, S. L., Briggs, K. H., Gourmelen, N., Graham, J. A., et al. (2017). Increased Ice Flow in Western Palmer Land Linked to Ocean Melting. *Geophys. Res. Lett.* 44, 4159–4167. doi:10.1002/2016gl072110

Ivins, E. R., James, T. S., Wahr, J., O. Schrama, E. J., Simon, K. M., and Simon, K. M. (2013). Antarctic Contribution to Sea Level Rise Observed by GRACE with Improved GIA Correction. *J. Geophys. Res. Solid Earth* 118, 3126–3141. doi:10.1002/jgrb.50208

Jacob, T., Wahr, J., Pfeffer, W. T., and Swenson, S. (2012). Recent Contributions of Glaciers and Ice Caps to Sea Level Rise. *Nature* 482, 514–518. doi:10.1038/nature10847

Jenkins, A., Shoosmith, D., Dutrieux, P., Jacobs, S., Kim, T. W., Lee, S. H., et al. (2018). West Antarctic Ice Sheet Retreat in the Amundsen Sea Driven by Decadal Oceanic Variability. *Nat. Geosci* 11, 733–738. doi:10.1038/s41561-018-0207-4

Joughin, I., Bindschadler, R. A., King, M. A., Voigt, D., Alley, R. B., Anandakrishnan, S., et al. (2005). Continued Deceleration of Whillans Ice Stream, West Antarctica. *Geophys. Res. Lett.* 32, n/a. doi:10.1029/2005gl024319

Joughin, I., Smith, B. E., and Medley, B. (2014). Marine Ice Sheet Collapse Potentially under Way for the Thwaites Glacier Basin, West Antarctica. *Science* 344, 735–738. doi:10.1126/science.1249055

Joughin, I., and Tulaczyk, S. (2002). Positive Mass Balance of the Ross Ice Streams, West Antarctica. *Science* 295, 476–480. doi:10.1126/science.1066875

Kaitheri, A., Mémin, A., and Rémy, F. (2021). Inter-Annual Variability in the Antarctic Ice Sheets Using Geodetic Observations and a Climate Model. *Remote Sensing* 13, 2199. doi:10.3390/rs13112199

Konrad, H., Gilbert, L., Cornford, S. L., Payne, A., Hogg, A., Muir, A., et al. (2017). Uneven Onset and Pace of Ice-dynamical Imbalance in the Amundsen Sea Embayment, West Antarctica. *Geophys. Res. Lett.* 44, 910–918. doi:10.1002/2016GL070733

Konrad, H., Shepherd, A., Gilbert, L., Hogg, A. E., McMillan, M., Muir, A., et al. (2018). Net Retreat of Antarctic Glacier Grounding Lines. *Nat. Geosci* 11, 258–262. doi:10.1038/s41561-018-0082-z

Lenaerts, J. T. M., van den Broeke, M. R., van de Berg, W. J., van Meijgaard, E., and Kuipers Munneke, P. (2012). A New, High-Resolution Surface Mass Balance Map of Antarctica (1979-2010) Based on Regional Atmospheric Climate Modeling: SMB ANTARCTICA. *Geophys. Res. Lett.* 39, n/a. doi:10.1029/2011gl050713

Levermann, A., Winkelmann, R., Albrecht, T., Goelzer, H., Golledge, N. R., Greve, R., et al. (2020). Projecting Antarctica's Contribution to Future Sea Level Rise from Basal Ice Shelf Melt Using Linear Response Functions of 16 Ice Sheet Models (LARMIP-2). *Earth Syst. Dynam.* 11, 35–76. doi:10.5194/esd-11-35-2020

Li, X., Rignot, E., Morlighem, M., Mouginot, J., and Scheuchl, B. (2015). Grounding Line Retreat of Totten Glacier, East Antarctica, 1996 to 2013. *Geophys. Res. Lett.* 42, 8049–8056. doi:10.1002/2015gl065701

Li, X., Rignot, E., Mouginot, J., and Scheuchl, B. (2016). Ice Flow Dynamics and Mass Loss of Totten Glacier, East Antarctica, from 1989 to 2015. *Geophys. Res. Lett.* 43, 6366–6373. doi:10.1002/2016GL069173

Lovell, A. M., Stokes, C. R., and Jamieson, S. S. R. (2017). Sub-decadal Variations in Outlet Glacier Terminus Positions in Victoria Land, Oates Land and George V Land, East Antarctica (1972-2013). *Antarctic Sci.* 29, 468–483. doi:10.1017/s0954102017000074

Lowry, D. P., Krapp, M., Golledge, N. R., and Alevropoulos-Borrill, A. (2021). The Influence of Emissions Scenarios on Future Antarctic Ice Loss Is Unlikely to Emerge This century. *Commun. Earth Environ.* 2, 221. doi:10.1038/s43247-021-00289-2

Mankoff, K. D., Solgaard, A., Colgan, W., Ahlstrøm, A. P., Khan, S. A., and Fausto, R. S. (2020). Greenland Ice Sheet Solid Ice Discharge from 1986 through March 2020. *Earth Syst. Sci. Data* 12, 1367–1383. doi:10.5194/essd-12-1367-2020

Martín-Español, A., King, M. A., Zammit-Mangion, A., Andrews, S. B., Moore, P., and Bamber, J. L. (2016). An Assessment of Forward and Inverse GIA Solutions for Antarctica. *J. Geophys. Res. Solid Earth* 121, 6947–6965.

Martinec, Z. (1989). Program to Calculate the Spectral Harmonic Expansion Coefficients of the Two Scalar fields Product. *Comput. Phys. Commun.* 54, 177–182. doi:10.1016/0010-4655(89)90043-X

Mémin, A., Flament, T., Alizier, B., Watson, C., and Rémy, F. (2015). Interannual Variation of the Antarctic Ice Sheet from a Combined Analysis of Satellite Gravimetry and Altimetry Data. *Earth Planet. Sci. Lett.* 422, 150–156. doi:10.1016/j.epsl.2015.03.045

Miles, B. W. J., Jordan, J. R., Stokes, C. R., Jamieson, S. S. R., Gudmundsson, G. H., and Jenkins, A. (2021). Recent Acceleration of Denman Glacier (1972-2017), East Antarctica, Driven by Grounding Line Retreat and Changes in Ice Tongue Configuration. *The Cryosphere* 15, 663–676. doi:10.5194/tc-15-663-2021

Morlighem, M., Rignot, E., Binder, T., Blankenship, D., Drews, R., Eagles, G., et al. (2020). Deep Glacial Troughs and Stabilizing Ridges Unveiled beneath the Margins of the Antarctic Ice Sheet. *Nat. Geosci.* 13, 132–137. doi:10.1038/s41561-019-0510-8

Mottram, R., Hansen, N., Kittel, C., van Wessem, M., Agosta, C., Amory, C., et al. (2020). What Is the Surface Mass Balance of Antarctica? an Intercomparison of Regional Climate Model Estimates. *Ice sheets/Antarctic*. doi:10.5194/tc-2019-333

Mouginot, J., Rignot, E., and Scheuchl, B. (2014). Sustained Increase in Ice Discharge from the Amundsen Sea Embayment, West Antarctica, from 1973 to 2013. *Geophys. Res. Lett.* 41, 1576–1584. doi:10.1002/2013gl059069

Nakayama, Y., Menemenlis, D., Zhang, H., Schodlok, M., and Rignot, E. (2018). Origin of Circumpolar Deep Water Intruding onto the Amundsen and Bellingshausen Sea continental Shelves. *Nat. Commun.* 9, 3403. doi:10.1038/s41467-018-05813-1

Nield, G. A., Barletta, V. R., Bordoni, A., King, M. A., Whitehouse, P. L., Clarke, P. J., et al. (2014). Rapid Bedrock Uplift in the Antarctic Peninsula Explained by Viscoelastic Response to Recent Ice Unloading. *Earth Planet. Sci. Lett.* 397, 32–41. doi:10.1016/j.epsl.2014.04.019

Nield, G. A., Whitehouse, P. L., King, M. A., and Clarke, P. J. (2016). Glacial Isostatic Adjustment in Response to Changing Late Holocene Behaviour of Ice Streams on the Siple Coast, West Antarctica. *Geophys. J. Int.* 205, 1–21. doi:10.1093/gji/ggv532

Paolo, F. S., Fricker, H. A., and Padman, L. (2015). Volume Loss from Antarctic Ice Shelves Is Accelerating. *Science* 348, 327–331. doi:10.1126/science.aaa0940

Parker, G. B., and Pryor, D. S. (1983). The Other Side of Statistical Significance. *Meteorol. Mag.* 13, 183. doi:10.1111/j.1445-5994.1983.tb02682.x

Payne, A. J., Nowicki, S., Abe-Ouchi, A., Agosta, C., Alexander, P., Albrecht, T., et al. (2021). Future Sea Level Change under Coupled Model Intercomparison Project Phase 5 and Phase 6 Scenarios from the Greenland and Antarctic Ice Sheets. *Geophys. Res. Lett.* 48, e2020GL091741. doi:10.1029/2020GL091741

Peltier, W. R., Argus, D. F., and Drummond, R. (2015). Space Geodesy Constrains Ice Age Terminal Deglaciation: The Global ICE-6G_C (VM5a) Model. *J. Geophys. Res. Solid Earth* 120, 450–487. doi:10.1002/2014JB011176

Reese, R., Gudmundsson, G. H., Levermann, A., and Winkelmann, R. (2018). The Far Reach of Ice-Shelf Thinning in Antarctica. *Nat. Clim Change* 8, 53–57. doi:10.1038/s41558-017-0020-x

Rignot, E., Bamber, J. L., Van Den Broeke, M. R., Davis, C., Li, Y., Van De Berg, W. J., et al. (2008). Recent Antarctic Ice Mass Loss from Radar Interferometry and Regional Climate Modelling. *Nat. Geosci* 1, 106–110. doi:10.1038/ngeo102

Rignot, E. J., Gogineni, S. P., Krabill, W. B., and Ekholm, S. (1997). North and Northeast Greenland Ice Discharge from Satellite Radar Interferometry. *Science* 276, 934–937. doi:10.1126/science.276.5314.934

Rignot, E., Mouginot, J., Morlighem, M., Seroussi, H., and Scheuchl, B. (2014). Widespread, Rapid Grounding Line Retreat of Pine Island, Thwaites, Smith, and Kohler Glaciers, West Antarctica, from 1992 to 2011. *Geophys. Res. Lett.* 41, 3502–3509. doi:10.1002/2014gl060140

Rignot, E., Mouginot, J., Scheuchl, B., Van den Broeke, M., van Wessem, M. J., and Morlighem, M. (2019a). Four Decades of Antarctic Ice Sheet Mass Balance from 1979-2017. *Proc. Natl. Acad. Sci. USA* 116, 1095–1103. doi:10.1073/pnas.1812883116

Rignot, E., Mouginot, J., Scheuchl, B., van den Broeke, M., van Wessem, M. J., and Morlighem, M. (2019b). Four Decades of Antarctic Ice Sheet Mass Balance from 1979-2017. *Proc. Natl. Acad. Sci. USA* 116, 1095–1103. doi:10.1073/pnas.1812883116

Rintoul, S. R., Silvano, A., Pena-Molino, B., van Wijk, E., Rosenberg, M., Greenbaum, J. S., et al. (2016). Ocean Heat Drives Rapid Basal Melt of the Totten Ice Shelf. *Sci. Adv.* 2, e1601610. doi:10.1126/sciadv.1601610

Sasgen, I., Groh, A., and Horwath, M. (2019a). GFZ GravIS RL06 Ice-Mass Change Products. *GFZ Data Serv.* 2. doi:10.5880/GFZ.GRAVIS_06_L3_ICE

Sasgen, I., Konrad, H., Helm, V., and Grosfeld, K. (2019b). High-Resolution Mass Trends of the Antarctic Ice Sheet through a Spectral Combination of Satellite Gravimetry and Radar Altimetry Observations. *Remote Sensing* 11, 144. doi:10.3390/rs11020144

Sasgen, I., Konrad, H., Ivins, E. R., Van den Broeke, M. R., Bamber, J. L., Martinec, Z., et al. (2013). Antarctic Ice-Mass Balance 2003 to 2012: Regional Reanalysis of GRACE Satellite Gravimetry Measurements with Improved Estimate of Glacial-Isostatic Adjustment Based on GPS Uplift Rates. *The Cryosphere* 7, 1499–1512. doi:10.5194/tc-7-1499-2013

Sasgen, I., Martín-Español, A., Horvath, A., Klemann, V., Petrie, E. J., Wouters, B., et al. (2017). Joint Inversion Estimate of Regional Glacial Isostatic Adjustment in Antarctica Considering a Lateral Varying Earth Structure (ESA STSE Project REGINA). *Geophys. J. Int.* 211, 1534–1553. doi:10.1093/gji/ggx368

Sasgen, I., Wouters, B., Gardner, A. S., King, M. D., Tedesco, M., Landerer, F. W., et al. (2020). Return to Rapid Ice Loss in Greenland and Record Loss in 2019 Detected by the GRACE-FO Satellites. *Commun. Earth Environ.* 1, 8. doi:10.1038/s43247-020-0010-1

Save, H., Bettadpur, S., and Tapley, B. D. (2016). High-resolution CSR GRACE RL05 Mascons. *J. Geophys. Res. Solid Earth* 121, 7547–7569. doi:10.1002/2016jb013007

Save, H. (2019). GRACE Follow-On CSR Level-2 Processing Standards Document. Available at: ftp://isdcftp.gfz-potsdam.de/grace-fo/DOCUMENTS/Level-2/GRACE-FO_CSR_L2_Processing_Standards_Document_for_RL06.pdf.

Scambos, T. A. (2004). Glacier Acceleration and Thinning after Ice Shelf Collapse in the Larsen B Embayment, Antarctica. *Geophys. Res. Lett.* 31, L18402. doi:10.1029/2004GL020670

Schannwell, C., Cornford, S., Pollard, D., and Barrand, N. E. (2018). Dynamic Response of Antarctic Peninsula Ice Sheet to Potential Collapse of Larsen C and George VI Ice Shelves. *The Cryosphere* 12, 2307–2326. doi:10.5194/tc-12-2307-2018

Scheuchl, B., Mouginot, J., and Rignot, E. (2012). Ice Velocity Changes in the Ross and Ronne Sectors Observed Using Satellite Radar Data from 1997 and 2009. *The Cryosphere* 6, 1019–1030. doi:10.5194/tc-6-1019-2012

Schröder, L., Horwath, M., Dietrich, R., Helm, V., van den Broeke, M. R., and Ligtenberg, S. R. M. (2019). Four Decades of Antarctic Surface Elevation Changes from Multi-mission Satellite Altimetry. *The Cryosphere* 13, 427–449. doi:10.5194/tc-13-427-2019

Selley, H. L., Hogg, A. E., Cornford, S., Dutrieux, P., Shepherd, A., Wuite, J., et al. (2021). Widespread Increase in Dynamic Imbalance in the Getz Region of Antarctica from 1994 to 2018. *Nat. Commun.* 12, 1133. doi:10.1038/s41467-021-21321-1

Seroussi, H., Nowicki, S., Payne, A. J., Goelzer, H., Lipscomb, W. H., Abe-Ouchi, A., et al. (2020). ISMIP6 Antarctica: a Multi-Model Ensemble of the Antarctic Ice Sheet Evolution over the 21st century. *The Cryosphere* 14, 3033–3070. doi:10.5194/tc-14-3033-2020

Shepherd, A., Gilbert, L., Muir, A. S., Konrad, H., McMillan, M., Slater, T., et al. (2019). Trends in Antarctic Ice Sheet Elevation and Mass. *Geophys. Res. Lett.* 46, 8174–8183. doi:10.1029/2019GL082182

Shepherd, A., Ivins, E., Rignot, E., Smith, B., van den Broeke, M., Velicogna, I., et al. (2018). Mass Balance of the Antarctic Ice Sheet from 1992 to 2017. *Nature* 558, 219–222. doi:10.1038/s41586-018-0179-y

Silva, A. B., Arigony-Neto, J., Braun, M. H., Espinoza, J. M. A., Costi, J., and Jaña, R. (2020). Spatial and Temporal Analysis of Changes in the Glaciers of the Antarctic Peninsula. *Glob. Planet. Change* 184, 103079. doi:10.1016/j.gloplacha.2019.103079

Smith, B., Fricker, H. A., Gardner, A. S., Medley, B., Nilsson, J., Paolo, F. S., et al. (2020). Pervasive Ice Sheet Mass Loss Reflects Competing Ocean and Atmosphere Processes. *Science* 368, 1239–1242. doi:10.1126/science.aaz5845

Sutter, J., Gierz, P., Grosfeld, K., Thoma, M., and Lohmann, G. (2016). Ocean Temperature Thresholds for Last Interglacial West Antarctic Ice Sheet Collapse. *Geophys. Res. Lett.* 43, 2675–2682. doi:10.1002/2016GL067818

Sutterley, T. C., Velicogna, I., Rignot, E., Mouginot, J., Flament, T., van den Broeke, M. R., et al. (2014). Mass Loss of the Amundsen Sea Embayment of West Antarctica from Four Independent Techniques. *Geophys. Res. Lett.* 41, 8421–8428. doi:10.1002/2014GL061940

Tapley, B. D., Bettadpur, S., Watkins, M., and Reigber, C. (2004). The Gravity Recovery and Climate Experiment: Mission Overview and Early Results. *Geophys. Res. Lett.* 31, L09607. doi:10.1029/2004gl019920

Tapley, B. D., Watkins, M. M., Flechtner, F., Reigber, C., Bettadpur, S., Rodell, M., et al. (2019). Contributions of GRACE to Understanding Climate Change. *Nat. Clim. Change* 9, 358–369. doi:10.1038/s41558-019-0456-2

Thomas, R., Scheuchl, B., Frederick, E., Harpold, R., Martin, C., and Rignot, E. (2013). Continued Slowing of the Ross Ice Shelf and Thickening of West Antarctic Ice Streams. *J. Glaciol.* 59, 838–844. doi:10.3189/2013jog12j122

Thompson, D. W. J., and Solomon, S. (2002). Interpretation of Recent Southern Hemisphere Climate Change. *Science* 296, 895–899. doi:10.1126/science.1069270

Tong, X., Liu, S., Li, R., Xie, H., Liu, S., Qiao, G., et al. (2018). Multi-track Extraction of Two-Dimensional Surface Velocity by the Combined Use of Differential and Multiple-Aperture InSAR in the Amery Ice Shelf, East Antarctica. *Remote Sensing Environ.* 204, 122–137. doi:10.1016/j.rse.2017.10.036

Trenberth, K. E. (1975). A Quasi-Biennial Standing Wave in the Southern Hemisphere and Interrelations with Sea Surface Temperature. *Q.J R. Met. Soc.* 101, 55–74. doi:10.1002/qj.49710142706

Turner, J., Lu, H., White, I., King, J. C., Phillips, T., Hosking, J. S., et al. (2016). Absence of 21st century Warming on Antarctic Peninsula Consistent with Natural Variability. *Nature* 535, 411–415. doi:10.1038/nature18645

Turner, J. (2004). The El Niño-Southern Oscillation and Antarctica. *Int. J. Climatol.* 24, 1–31. doi:10.1002/joc.965

van Wessem, J. M., van de Berg, W. J., Noël, B. P. Y., van Meijgaard, E., Amory, C., Birnbaum, G., et al. (2018). Modelling the Climate and Surface Mass Balance of Polar Ice Sheets Using RACMO2 - Part 2: Antarctica (1979-2016). *The Cryosphere* 12, 1479–1498. doi:10.5194/tc-12-1479-2018

Velicogna, I., Mohajerani, Y., A, G., Landerer, F., Mouginot, J., Noel, B., et al. (2020). Continuity of Ice Sheet Mass Loss in Greenland and Antarctica from the GRACE and GRACE Follow-On Missions. *Geophys. Res. Lett.* 47, e2020GL087291. doi:10.1029/2020GL087291

WCRP Global Sea Level Budget Group (2018). Global Sea-Level Budget 1993–present. *Earth Syst. Sci. Data* 10, 1551–1590. doi:10.5194/essd-10-1551-2018

Wouters, B., Bamber, J. L., Van den Broeke, M. R., Lenaerts, J. T. M., and Sasgen, I. (2013). Limits in Detecting Acceleration of Ice Sheet Mass Loss Due to Climate Variability. *Nat. Geosci* 6, 613–616. doi:10.1038/ngeo1874

Wouters, B., Gardner, A. S., and Moholdt, G. (2019). Global Glacier Mass Loss during the GRACE Satellite Mission (2002-2016). *Front. Earth Sci.* 7, 96. doi:10.3389/feart.2019.00096

Wouters, B., Martin-Español, A., Helm, V., Flament, T., van Wessem, J. M., Ligtenberg, S. R. M., et al. (2015). Dynamic Thinning of Glaciers on the Southern Antarctic Peninsula. *Science* 348, 899–903. doi:10.1126/science.aaa5727

Yuan, D.-N. (2019). GRACE Follow-On JPL Level-2 Processing Standards Document for Level-2 Product Release 06. Available at: http://icgem.gfz-potsdam.de/GRACE-FO_JPL_L2_Processing_Standards_Document_for_RL06.pdf.

Zhang, B., Yao, Y., Liu, L., and Yang, Y. (2021). Interannual Ice Mass Variations over the Antarctic Ice Sheet from 2003 to 2017 Were Linked to El Niño-Southern Oscillation. *Earth Planet. Sci. Lett.* 560, 116796. doi:10.1016/j.epsl.2021.116796

**Conflict of Interest:** The authors declare that the research was conducted in the absence of any commercial or financial relationships that could be construed as a potential conflict of interest.

**Publisher's Note:** All claims expressed in this article are solely those of the authors and do not necessarily represent those of their affiliated organizations, or those of the publisher, the editors and the reviewers. Any product that may be evaluated in this article, or claim that may be made by its manufacturer, is not guaranteed or endorsed by the publisher.